# Long-term hazard assessment of explosive eruptions at Jan Mayen Island (Norway) and implications on air-traffic in the North Atlantic

Manuel Titos[1], Beatriz Martinez Montesinos[2], Sara Barsotti[1], Laura Sandri[2], Arnau Folch[3,4], Leonardo Mingari[3], Giovanni Macedonio[5], and Antonio Costa[2]

[1]Icelandic Meteorological Office (IMO), Iceland
[2]Istituto Nazionale di Geofisica e Vulcanologia, Sezione di Bologna, Italy
[3]Barcelona Supercomputing Center (BSC), Spain
[4]Geociencias Barcelona, Consejo Superior Investigaciones Cientificas, (CSIC), Spain
[5]Istituto Nazionale di Geofisica e Vulcanologia, Osservatorio Vesuviano, Italy

**Correspondence:** Manuel Titos (manuel@vedur.is)

**Abstract.** Volcanic eruptions are amongst the most jeopardizing natural events due to their potential impacts on life, assets, and environment. In particular, atmospheric dispersal of volcanic tephra and aerosols during the explosive eruptions poses a serious threat to life and has significant consequences for infrastructures and global aviation safety. The volcanic island of Jan Mayen, located in the North Atlantic under trans-continental air traffic routes, is considered the northernmost active volcanic area in the world, with at least 5 eruptive periods recorded during the last 200 years. However, quantitative hazard assessments on the possible consequences for air traffic of a future ash-forming eruption at Jan Mayen are nonexistent. This study presents the first comprehensive long-term volcanic hazard assessment for Jan Mayen volcanic island in terms of ash dispersal and concentration at different flight levels. In order to delve in the characterization and modelling of that potential impact, a probabilistic approach based on merging a large number of numerical simulations is adopted, varying the volcano's Eruption Source Parameters (ESPs) and meteorological scenario. Each ESP value is randomly sampled following a continuous Probability Density Function (PDF) based on the Jan Mayen geological record. Over 20 years of meteorological data are considered in order to explore the natural variability associated with weather conditions and used to run thousands of simulations of the ash dispersal model FALL3D on a 2 km-resolution grid. The simulated scenarios are combined to produce probability maps of airborne ash concentration, arrival time and persistence of unfavorable conditions at flight levels 50 and 250 (FL050 and FL250). The resulting maps can represent an aid to civil protection, decision makers and, moreover, aviation stakeholders in assessing and preventing the potential impact from a future ash-rich eruption at Jan Mayen.

## 1 Introduction

Along with earthquakes, tsunamis and weather extremes, explosive volcanic activity is amongst the most threatening natural hazards, with potential to contribute to global warming and environmental changes (Ward, 2015). The impacts of volcanic emissions can extend over large distances from the source, posing a threat to human health and jeopardizing air navigation. Some recent examples of events leading to millionaire losses due to air traffic disruption include the eruptions in Eyjafjallajökull (Ice-

land, 2010), Grímsvötn (Iceland, 2011) and Puyehue-Cordón Caulle (Chile, 2011) (Mazzocchi et al., 2010; Oxford-economics, 2010; Tesche et al., 2012; Karlsdóttir et al., 2012; Budd et al., 2011; Elissondo et al., 2016). These events were a stark reminder on the importance of volcanic hazard assessment and related quantification of impacts of future eruptions, both essential tools to advise governments, aviation stakeholders and the society in general, contributing, in this way, to their preparedness. In 2019, before the COVID-19 pandemics aviation break, Icelandic airports received around 8M passengers (7M international and 0.7M domestic) on a total of 181k flights (Isavia, 2019). In turn, polar air traffic routes had shown a marked increase over the last years, with a 15-fold increase between 2003 and 2015, and reaching more than 14k flights yearly since 2016 (Nav-Canada, 2017; Stewart-Green, 2016).

Although Jan Mayen (JM) volcano tephrochronology reveals at least 8 eruptive periods over the last 600 years, 5 of them concentrated in the last 200 years (Gjerløw et al., 2016), the potential impact on air traffic following a future ash-forming eruption has never been assessed. According to Gjerløw et al. (2016), the most likely volcanism at JM island is characterized by effusive Hawaiian to violent Strombolian eruptions and, to a lesser extent, by lava domes and Surtseyan eruptions. However, due to the possibility of magma interacting with sea water, snow or ice, the likelihood of moderately to highly explosive eruptions is considerable. Historical distal records of trachytic tephra found in Ireland (Hunt, 2004) and basaltic tephra found in older sedimentary records in the North-Atlantic (Lacasse and Garbe-Schönberg, 2001; Brendryen et al., 2010; Voelker and Haflidason, 2015) or in Greenland ice-cores (Abbott and Davies, 2012) show the potential for producing Plinian explosive eruptions, whose size and frequency are, however, highly uncertain.

This paper presents the first comprehensive long-term Probabilistic Volcanic Hazard Assessment (PVHA) for JM volcanic island focused on the potential impact of airborne tephra concentration on arctic and north-Atlantic air routes. This is done by using the FALL3D model (Folch et al., 2009, 2020) to simulate the transport of ash clouds and its concentration at two relevant flight levels over a geographical area of approx 2000 km x 2000 km covering Iceland and the U.K.

In order to account for the natural variability in volcanic eruption intensity, vent position and wind field, two main steps have been followed as suggested in Sandri et al. (2016).

First, based on field data, we identify the possible eruptive classes for JM volcano and then we define a Probability Density Function (PDF) to describe the relative probability of the different classes to occur. For each class, we then define PDFs for each eruptive parameter (such as eruption duration or total erupted mass) in order to account for the natural variability of the eruption conditions. Then, by randomly sampling these PDFs, we generate a large dataset of ESP to be used as model input. A novel strategy is proposed to treat and describe the styles of pulsating eruptions, characterized by a series of discrete short-lived events followed by occasional interruption of tephra emission. Secondly, to fully explore the natural variability of the meteorological conditions, the numerical simulations have been randomly initialized within the period 1999-2020 (21 years). The meteorological data have been obtained from ERA5 reanalysis dataset and FALL3D used to generate thousands simulations per representative eruptive scenario. As a result, the following questions are answered:

- which is the probability that, in case of an eruption at JM, the ash cloud concentration will exceed the critical condition for safe flights within a domain extending down to the U.K. airspace after 3, 6, 12, 24 hours since the beginning of the eruption?

- in case of an eruption at JM, which is the probability that airports in Iceland and U.K. will be affected by the presence of ash?
- which is the probability to exceed a predefined hazardous temporal persistence of unsafe flight conditions?
- which flight level (FL) is likely to be predominantly affected by critical concentrations of volcanic ash?

The rest of the paper is organized as follows: Section 2 provides a historical overview of the Holocene volcanic activity of JM volcano. Section 3 describes the most likely eruptive classes based on the five historical known eruptions of JM, fits them into a PDF for the total erupted volume, addresses a novel strategy to treat and describes the styles of pulsating eruptions. Sections 4 and 5 present results and discussions, and finally, Section 6 concludes the study.

## 2 Jan Mayen Volcanism

JM is a Norwegian volcanic island located in the North-Atlantic Ocean at 71° N, 8° W around 600 km North of Iceland, in the Norwegian Greenland Sea (Fig. 1). According to Kandilarov et al. (2012); Larsen et al. (2021), Jan Mayen microcontinent (JMMC, Fig. 2a) is a structural entity enclosing the Jan Mayen Ridge (JMR) and the surrounding area, including the Jan Mayen Basin (JMB), the Jan Mayen Basin South (JMBS), the Jan Mayen Trough (JMT), and the Southern Ridge Complex (SRC) (see Fig. 2b). To the north, JMMC is bordered by the Jan Mayen Fracture Zone (JMFZ) and the volcanic complex of Jan Mayen Island, while to the South, East and West it borders by the NE coastal shelf of Iceland (NIS), the Norway Basin and the Kolbeinsey Ridge (KBR), respectively (Fig. 2a). Although the historic activity reports at least five eruptive periods over the last 200 years (since the discovering of the island at the beginning of the 17th century) (Gjerløw et al., 2016), its Holocene eruptive history is basically unknown. In this sense, the eruptive history of JM comprises only a very few distal sediment cores as well as lava flows and tephra deposits from eruptions on the ice-free parts of the Beerenberg volcano. Distal records as trachytic tephra found in Ireland (Hunt, 2004) and basaltic tephra found in older sediment-records in the North-Atlantic (Lacasse and Garbe-Schönberg, 2001; Brendryen et al., 2010; Voelker and Haflidason, 2015) or in Greenland ice-cores (Abbott and Davies, 2012) have shown the potential for explosive ash-forming eruptions whose size, frequency, and potential impact are, however, uncertain. According to Imsland (1978), explosive hydromagmatic eruptions were common earlier in the history of JM. Nevertheless, as the island grew above sea level, such eruptions became less frequent and the volcanism essentially localized on two different regions: 1) the Beerenberg central volcano and its flank eruptions in northeastern part (called Nord-Jan) and, 2) the volcanic ridge extending from the middle to the southwestern part (called Midt-Jan and Sør-Jan respectively). On one hand, considering that the higher altitudes of the volcano are ice-covered and glacier tongues extend down to sea level at several locations, the Holocene eruptions from the summit crater are difficult to map and no tephra layers have been positively linked to eruptions from the summit. Only a few land-based tephra records on the ice-free areas of Beerenberg have been mapped with some detail. Based on several sediment cores, Gjerløw et al. (2016) concludes that the Holocene volcanism on Beerenberg has been effusive or mildly explosive. As a result, the most common forms of recognized volcanic activity at Beerenberg are flank eruptions in the form of basaltic fissure and Strombolian to violent Strombolian eruptions. Eruption

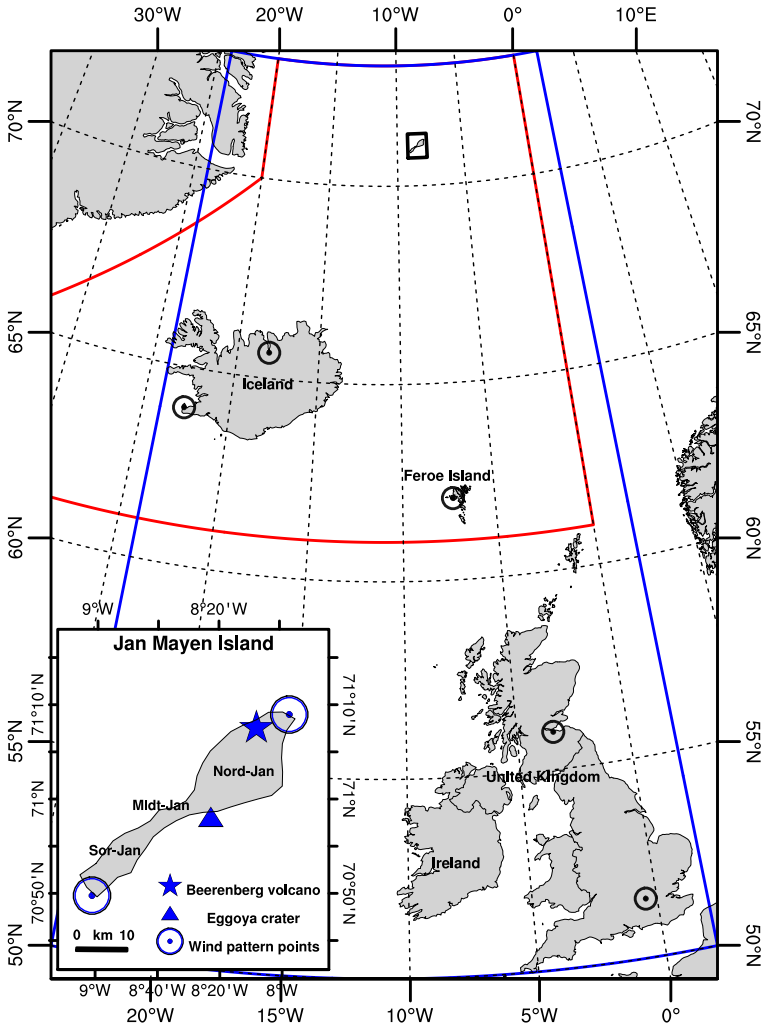


**Figure 1.** JM location and computational domain for the JM PVHA including Iceland, Ireland, and the United Kingdom (blue box). The red contour shows the FIR (Flight Information Region) for which Icelandic Meteorological Office is responsible (for visualization purposes only). The blue star and triangle in the zoomed map indicate the location of Beerenberg volcano and Eggoya crater (1732 Surtseyan eruption) respectively. The 2 blue circles show the 2 hypothetical vent locations in the wind profile analysis. Black circles correspond to Keflavik and Akureyri (Iceland), Vágar (Faroe Islands), Edinburgh (Scotland) and Heathrow (U.K., London) airports. Nord-Jan, Midt-Jan and Sør-Jan correspond to 3 areas in which JM is classically divided.

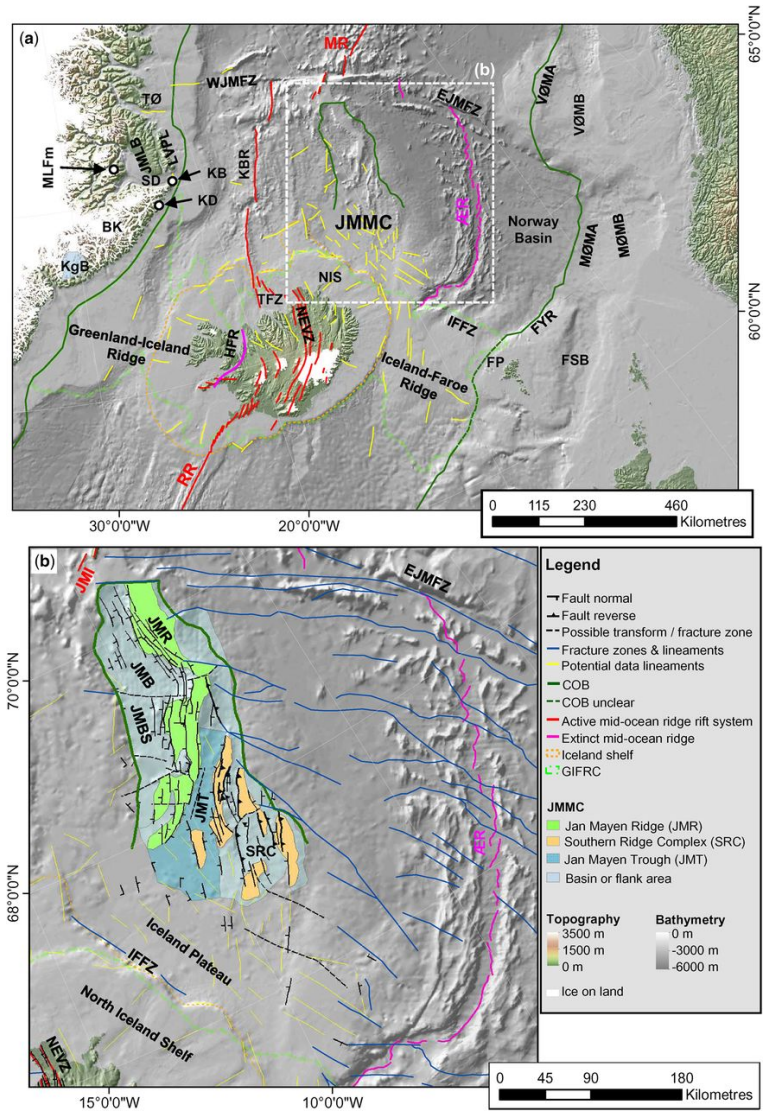


**Figure 2.** Overview map (a) of the study area with the location of structural elements identified on potential field data. Structural elements map (b) for the Jan Mayen microcontinent (JMMC): mapped faults, fractures zones and lineaments based on Peron-Pinvidic et al. (2012); Gernigon et al. (2015). The background image is shaded bathymetry (IBCAO 3.0: (Jakobsson et al., 2012; Amante and Eakins, 2009)). Image retrieved from Blischke et al. (2017).

**Table 1.** Possible relative eruption scenarios on JM Island. The categorization is based on the volume of tephra emitted in DRE. Data obtained from Larsen and Guðmundsson (2016); Gjerløw et al. (2016). According to the geological record (extending beyond the Holocene), subPlinian/Plinian events are highy unlikely (1%). Because of this, they are not included in this table.

| | Total Erupted Volume ($km^3$ (DRE)) | Eruption Magnitude | Eruption type (VEI) | Duration (hour/days) | Historical relative frequency (Probability) |
|---|---|---|---|---|---|
| Small | <0.1 | 1 to 2 | small lava flows or small scoria cones. VEI=2 | 35-40 hours | 1 out 5 (20%) |
| Medium | 0.1-0.5 | 3 to 4 | Effusive and/or Vulcanian to violent Strombolian Surtseyan. VEI=3 | 4-40 days possibly pulsating if Surtseyan | 2-3 out 5 (40-60%) |
| Large | >0.5 | 4 to 5 | Explosive and/or effusive VEI=4 | 1-5 days | 1-2 out 5 (20-40%) |

frequency is difficult to assess due to scarce reconstruction data. However, during historical times, the Beerenberg's eruption rate has been around 1 eruption every 60-70 years, with eruptive phases lasting in the range of days to months. During the most recent effusive eruption in 1970, the largest known one during the Holocene, the volume of lava flows was of at least 0.5 $km^3$ Dense Rock Equivalent (DRE) (Siggerud, 1972). On the other hand, volcanism on Midt-Jan and Sør-Jan represents mostly effusive eruptions characterized by scoria cones, shallow marine to coastal phreatomagmatic eruptions, coulees and domes (Larsen and Guðmundsson, 2016; Gjerløw et al., 2015). The eruption frequency on this part of JM is also difficult to assess due to erosion and superimposition of newer vents (possibly covering and removing older ones). However, considering visible evidence, the (under) estimated number of eruptions over the last 10k years is around 45, resulting in an eruption frequency of 1 eruption every 220 years. The duration of the eruptions from Midt and Sør-Jan is still unknown. The unrest episode recorded in 1732 (Eggoya, Midt-Jan), which led to the largest known explosive eruption, was a Surtseyan eruption that dispersed tephra over large parts of JM and the surrounding seas. The volume of tephra ranges between 0.3-0.4 $km^3$ (Gjerløw et al., 2015).

## 3 Methodology

### 3.1 Eruption scenarios

Despite the limitations of a complete geological record composed of both chronological and statistical data, the possible relative eruptive scenarios at JM are based on 5 historical and prehistorical known eruptions. According to the categorization proposed by Larsen and Guðmundsson (2016); Gjerløw et al. (2016), eruption scenarios can be characterised by small ($< 0.1$ $km^3$), moderate (0.1-0.5 $km^3$), large ($> 0.5$ $km^3$) DRE volumes or magnitudes (see Table 1) (Pyle, 2015), and sub-Plinian eruptions.

– Small eruptions are mostly effusive events characterised by small lava flows or small scoria cones, with erupted volumes ranging $10^7$-$10^8$ m$^3$ (total less than 0.1 km$^3$ DRE), corresponding to eruption magnitudes 1 to 2, hence VEI=2 (Newhall and Self, 1982). Based on historical occurrence, this scenario can last for about 35-40 hours.

– Medium eruptions include subaerial, sub-glacial and even Surtseyan eruptions depending on within which environment they occur. Subaerial eruptions would be mainly located on Beerenberg volcano and they are expected to be effusive and/or Vulcanian to violent Strombolian. When effusive, medium eruptions are characterised by aa-lavas but also pahoehoe-flows. Surtseyan eruptions are expected to be located on JM and the surrounding shallow part of the ocean. These eruptions consist of phreatomagmatic pulses, each of which, according to observations, can last for approximately 0.5-8 days, generate a volcanic plumes between 3 and 11 km above sea level (a.s.l), and have a range of total erupted volume of $10^8$ –$10^{8.7}$ m$^3$ (0.1-0.5 km$^3$ DRE), corresponding to eruption magnitudes 3 to 4, and VEI=3. The total duration of the eruption is not well constrained, as it can last between approximately 4 days and 1 month. As a result, tephra-forming phases are expected, producing deposits more than one-meter thick within 5 km from the vent. The reference eruption for the Surtseyan type is the Eggoya 1732 AD eruption that produced at least 0.3-0.4 km$^3$ of tephra (0.16-0.21 km$^3$ DRE) (Gjerløw et al., 2015, 2016).

– Large eruptions are expected to be initially subglacial and include moderate to sub-Plinian eruptions. During the opening phases, due to magma-ice interaction, the activity is explosive and characterised by plume heights reaching more than 10 km a.s.l and a range of total erupted volume of $10^{8.7}$–$10^9$ m$^3$ (total volume emitted $>$ 0.5 km$^3$ DRE), corresponding to eruption magnitudes of 4 to 5 and VEI=4. In this initial short-lasting explosive phase, a very small amount of tephra is expected to be ejected (approximately 5% of the total erupted mass). The reference eruption for this type is the 1970 event that produced at least 0.5 km$^3$ DRE (Siggerud, 1972). As the eruption proceeds it becomes more effusive lasting for 1-4 days.

– Very Large eruptions include sub-Plinian to Plinian eruptions characterised by column heights from 15 km to 25 km a.s.l and a range of total erupted volume of $10^9$–$10^{9.7}$ m$^3$, hence eruption magnitudes of 5 to 6, corresponding to sub-Plinian type I or VEI $\geq$5. According to Gjerløw et al. (2016), in the geological record (extending beyond Holocene) there is evidence of 10 tephra layers from subPlinian/Plinian events in 119k years. Because of this, we assign a subjective probability of 1% to this class in case of eruption.

### 3.2 Probabilistic hazard assessment approach

Until a few years ago, volcanic hazard assessment was largely based on the concept of "eruptive scenario", characterized by subjectively-defined eruption conditions. Hazard was then quantified under the strong assumption that the next eruption from a given volcano will be similar to the selected "representative eruptive scenario" (Macedonio et al., 2008; Barsotti et al., 2018). However, when assuming a representative eruptive scenario, one is implicitly neglecting the large uncertainties (both aleatory and epistemic) in the parameters that define the scenario also called "intra-size variability" (Woodhouse et al., 2015;

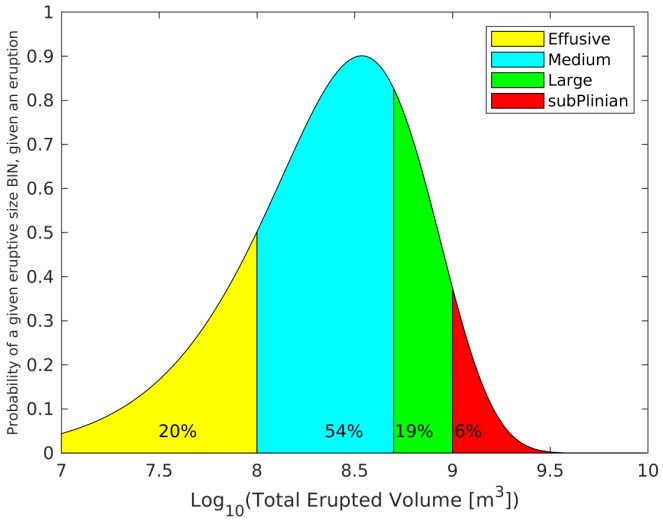


**Figure 3.** Weibull PDF describing the conditional probability of different eruptive magnitudes in case of an eruption at JM Island. The four colors cover the erupted volume ranges in the four "classical" eruption classes for JM, classically synthesized in 4 representative scenarios with a fixed mass, neglecting the variability in volume around these scenarios. The area under the different parts of the plot correspond to the probability of an Effusive, Medium, Large and subplinian class range eruption respectively, conditional to eruption occurrence. These values are in agreement with previous studies for JM (Larsen et al., 2017; Gjerløw et al., 2016).

Harvey et al., 2018). More recent approaches try to circumvent the effects of natural variability by averaging hundreds of simulations where eruption parameters are sampled within a broad set of eruptive conditions in the so-called "eruption range scenarios" (Bonadonna et al., 2005; Folch and Sulpizio, 2010; Prata et al., 2019). However, the use of a specific and limited range of eruption parameters continues introducing a large biased and uncertainties in the description of potential eruptive processes. For this reason, more recent approaches are based on the concept of a continuum of possible combinations of eruptive parameters, which translates into exploring a large set (many thousands) of simulations as proposed by Sulpizio et al. (2012); Sandri et al. (2016). Eruption parameters (e.g, total erupted mass, duration of the fallout phase, mass eruption rate, total grain size distribution, etc.) are defined and randomly sampled from specific probability distributions (Sandri et al., 2016). The processes for sampling and weighting possible statistical combinations of values for the volcanological parameters corresponds to their probability of occurrence: this allows giving more/less weight to more/less likely combinations. In order to explore the intra-size variability, we proceed as in Sandri et al. (2016):

1. A very broad range of possible eruptive scenarios, characterized by the total erupted volume, is selected as explained in Section 3.1.

2. The total erupted volume is used to define the total erupted mass, the eruption magnitude, and the VEI.

3. The eruptive range is split into eruption classes linked to representative members (see Section 3.1), each characterized by an approximate conditional probability in the geological and historical record (see Table 1).

4. Over the total range of possible erupted volumes (approximately $10^7 - 10^{10}$ m$^3$), up to 6 different truncated Probability Density Functions (PDF) are tested to describe the conditional probability of these 4 mutually exclusive classes: Normal, Exponential, LogLogistic, LogNormal, Gamma and Weibull. The best model is selected according to the Akaike's Information Criterion (AIC) (Bozdogan, 1987; Akaike, 1998), where the relative goodness of fit of such PDFs (i.e., the likelihood of the catalog's frequencies of the different eruptive classes, under different PDFs) is compared, penalized by the number of parameters. The PDF with the lowest AIC is considered the best among all specified ones. Indeed, the assumption of a common PDF for the total erupted volume across the different eruption classes allows a smooth and coherent linking among them (Sandri et al., 2016). For JM, the Weibull PDF better fitted the expected frequencies on the sub-ranges for the 4 different eruption classes. This PDF is used to assign a conditional probability of occurrence to each simulation as a function of the associated total erupted volume (see Figure 3).

5. Considering the behavior of similar scenarios including wet plumes, for Medium and Large classes we account for ash aggregation assuming two different aggregate types characterised by densities in the range of 250 and 350 kg/m$^3$ and diameters between 100 and 250 $\mu$m.

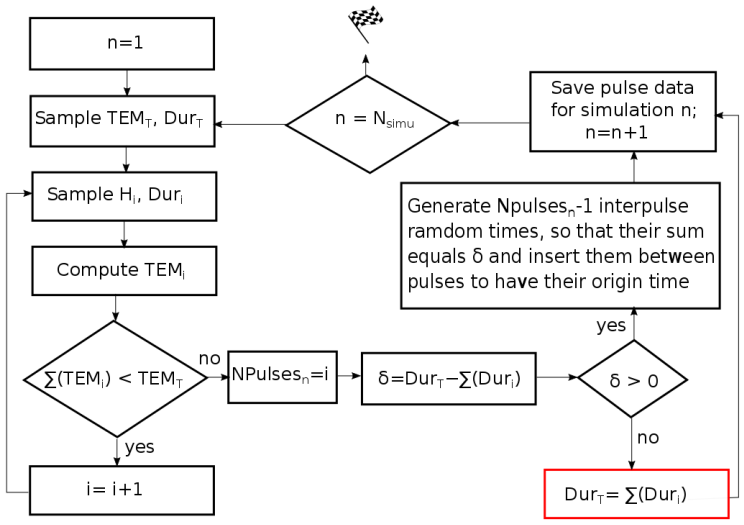


**Figure 4.** Proposed strategy to treat and describe the styles of pulsating eruptions, characterized by a series of discrete short-lived events followed by occasional interruption of the tephra emission.

### 3.3 Pulsating eruptions: Modelling and strategy

A novel strategy is proposed to describe the styles and model dispersal from pulsating eruptions (Surtseyan eruptions, belonging to Medium class in Table 1), characterized by a series of discrete short-lived events followed by occasional interruption of the emission of tephra. The strategy has been developed considering the ranges of all the ESP described in Section 3.1. For each pulsating scenario, the ESP associated with column shape, total grain size distribution, and sphericity of tephra particles are also sampled from given PDFs. However, the difference is that column heights are not derived from the mass eruption rate but using the following approach (see Figure 4):

1. Sampling randomly both the total erupted mass ($\text{TEM}_T$) and total duration of the eruption ($\text{Dur}_T$) considering values reflected in Section 3.1.

2. If the sum of masses erupted by all pulses does not equal or exceed the total erupted mass previously sampled, loop to:

   - Create the $i-th$ pulse sampling randomly column height ($\text{H}_i$) and duration ($\text{Dur}_i$). The duration is sampled from a normal distribution consistent with the data reflected in Table 1. The column height is sampled from a triangular distribution with lower limit 3 km, peak at 6 km, and upper limit 11 km a.s.l.
   - Compute the total erupted mass for such pulse ($\text{TEM}_i$) using the Mastin et al. (2009) relationship.
   - Compute ($\sum_{i=1}^{n}(\text{TEM}_i)$), being $n$ the number of pulses generated so far:
     - If ($\sum_{i=1}^{n}(\text{TEM}_i)) > 0.97*\text{TEM}_T$ and ($\sum_{i=1}^{n}(\text{TEM}_i)) < \text{TEM}_T$), modify $\text{TEM}_i$ to obtain $\sum_{i=1}^{n}(\text{TEM}_i) = \text{TEM}_T$, thereby avoiding small pulses. Compute the new column height ($\text{H}_i$) using Mastin et al. (2009).
     - Else, if total erupted mass obtained ($\sum_{i=1}^{n}(\text{TEM}_i)) < \text{TEM}_T$, save the pulse. Otherwise, discard the pulse.

3. Compute the duration of the eruption as the sum of the duration of all the pulses ($\sum_{i=1}^{n}(Dur_i)$). If the $\sum_{i=1}^{n}(Dur_i) < Dur_T$, generate n-1 inter-pulses at random time ($Res_i$) so that their sum equals $\delta$ ($\delta$=$Dur_T - \sum_{i=1}^{n}(Dur_i)$) and insert them between pulses. Otherwise, if $\sum_{i=1}^{n}(Dur_i) > \text{Dur}_T$, update $\text{Dur}_T$ = $\sum_{i=1}^{n}(Dur_i)$. This case actually supposes a continuous eruption where each pulse occurs without a rest period.

### 3.4 Vent location sensitivity

Given the scales of JM Island and the considered domain, the effects of the uncertain vent location on the resulting long-range hazard assessment can be expected to be negligible. In order to check this assumption we inspected how ERA5 wind profiles vary along the island by focusing on 2 vent locations at the NE (71.15º N, 7.95º W) and SW (70.82º N, 9.02º W) edges of the island, approximately 55 km apart (blue circles in Figure 1 inset). At these locations we inspected:

- Local wind profiles: Figure 5 shows vertical profiles of wind speed and direction averaged for the whole month of December, 2019. As observed, there are little differences in patterns between the two locations.

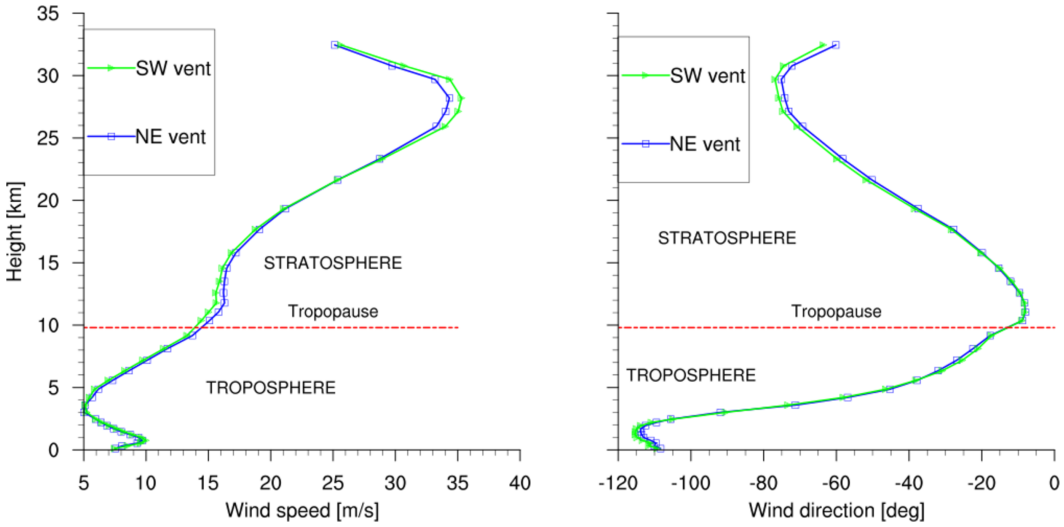


**Figure 5.** Monthly averaged ERA5 wind profiles (speed and direction) at 2 different locations (NE and SW) of JM Island.

– Annual wind profiles: Figure 6 shows the wind profiles averaged monthly for the year 2018. Once again, there are no differences between the two locations.

Considering the current limitation of both grid resolution and meteorological data resolution, the location of potential JM vents does not influence the ash dispersal pattern. As a result, we will not consider the uncertainty on the vent location and assume a fixed vent in the middle of the island.

## 4 Results: Hazard maps and uncertainty quantification

Hazard and probability maps (Elefante et al., 2010) are powerful tools to inform on spatial and temporal potential impact of specific volcanic phenomena. Commonly, they consist of exceedance probability curves, referred to as hazard curves (Hill et al., 2013). These hazard curves quantify, in a grid point of the target domain and within a specific time window (exposure time) (Budnitz et al., 1997), the exceedance probability of an intensity measure threshold for a specific phenomenon (e.g., tephra load at ground level or airborne tephra concentration).

Our objective is to show the usefulness of probabilistic volcanic hazard assessment in the framework of High Performance Computing evaluating the impact of low-probability but high-consequence events on air traffic (between Iceland and U.K., see Figure 1) from a potential eruption at JM Island, while quantifying how the ESP and wind patterns (velocity and direction) influence hazard and probability maps of ash dispersal and airborne tephra concentration.

Although our method allows analyzing any desired FL, in this work, only FL050 and FL250 (approx. 1.5 and 7.5 km a.s.l) will be analyzed. Such FLs were motivated considering standard cruise and maximum risk actions altitudes like takeoff or

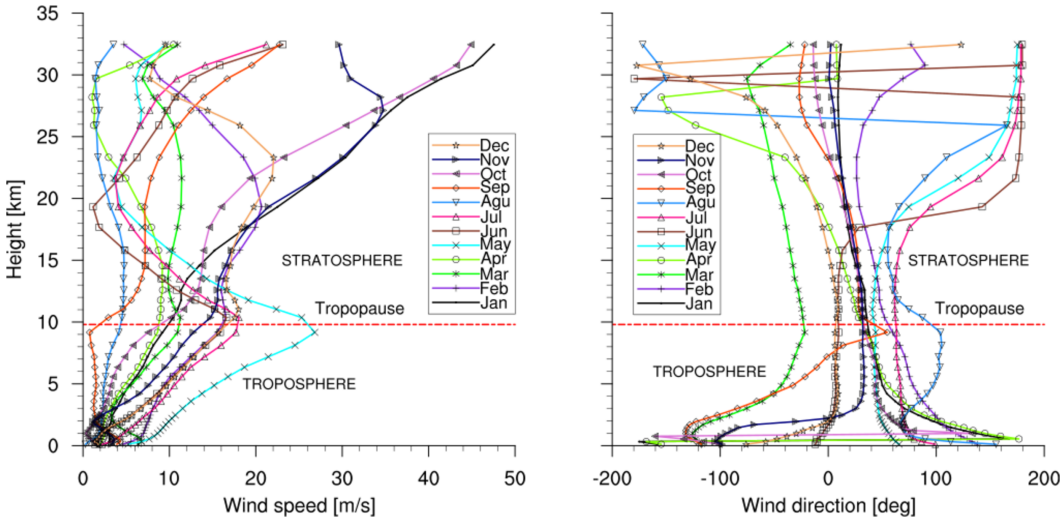


North-East vent

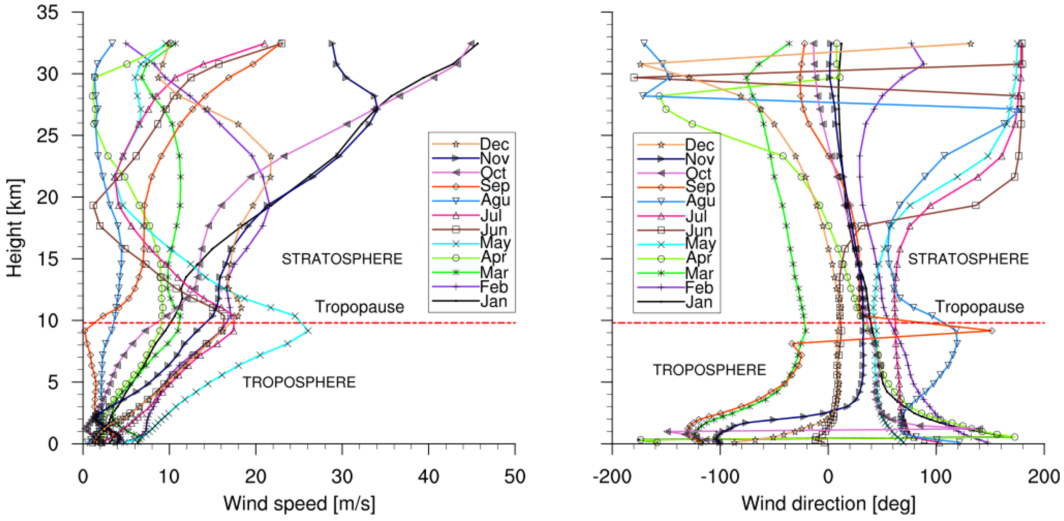


South-West vent

**Figure 6.** Monthly comparison of the wind pattern computed in 2 different locations (NE and SW) for a whole year, 2018. Top: Wind patterns corresponding to NE vent. Bottom: Wind patterns corresponding to SW vent. Results were obtained by averaging one year of ERA5 data.

landing. Finally, three selected ash concentration thresholds (0.2, 2, and 4 mg/m$^3$) were selected based on the impacts of volcanic ash on jet engines summarized in Figure 7 and the considerations included in the Volcanic Ash Contingency Plan published by the International Civil Aviation Organization (ICAO, 2021). As a result, we analyze the results using isolines at FL050 and FL250 for these three selected ash concentration thresholds through three different types of probabilistic maps:

- **Arrival time maps**: expected time required for the ash concentration to exceed 2 mg/m$^3$ at FL050 with an exceedance probability of 5%, between 0 and 48 hours since the beginning of the eruption.

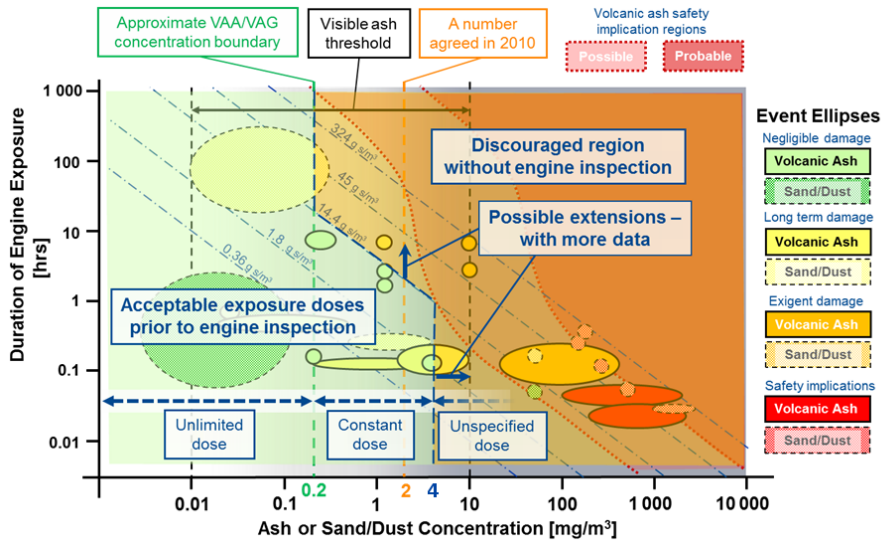


**Figure 7.** Overview of volcanic ash or sand/dust impacts on Jet Engines. Modified from Rolls-Royce review of aircrafts encountering airborne particle clouds (Ellis et al., 2021; Clarkson et al., 2016).

- **Exceedance probability maps**: reporting the probability of reaching ash concentration above a given threshold (0.2, 2, and 4 mg/m$^3$) at FL050 and FL250 at some time from the onset of the eruption up to 48 hours after its end.

- **Persistence maps**: showing the fraction of hours (since the beginning of the eruption) during which the ash concentration exceeds a given threshold (0.2, 2 and 4 mg/m$^3$) with a probability larger than 5%.

Figure 8 depicts the arrival time maps for Large and Medium eruptions respectively. The % value in exceedance probability has been subjectively selected. However we highlight that our method allows a potential end user to explore any value of exceedance probability: here, we only show the 5% maps as an example.

Figures 9 and D1 in the Appendix D show the probability of reaching or exceeding ash concentration above 0.2 mg/m$^3$, 2 mg/m$^3$, and 4 mg/m$^3$ at FL050 and FL250 at some time from the onset of the eruption up to 48 hours after its end for Large and Medium eruptive classes respectively.

Thousands of eruptive scenarios have been simulated to reproduce and capture, in a probabilistic way, the variability of a phenomena which can vary strongly in space and time. However, a proper uncertainty quantification (UQ) is needed to quantify how reliable the prediction is. Such UQ can provide useful knowledge about the diversity of the dominant winds, the range in the airborne tephra concentration and its extent depending on the type of eruption, the ESP related to the eruption size, and the feature of pulsating events for Medium size eruptions. As a consequence, the threat evaluation and the spatio-temporal analysis presented here could bring forth a more robust comprehensive hazard assessment.

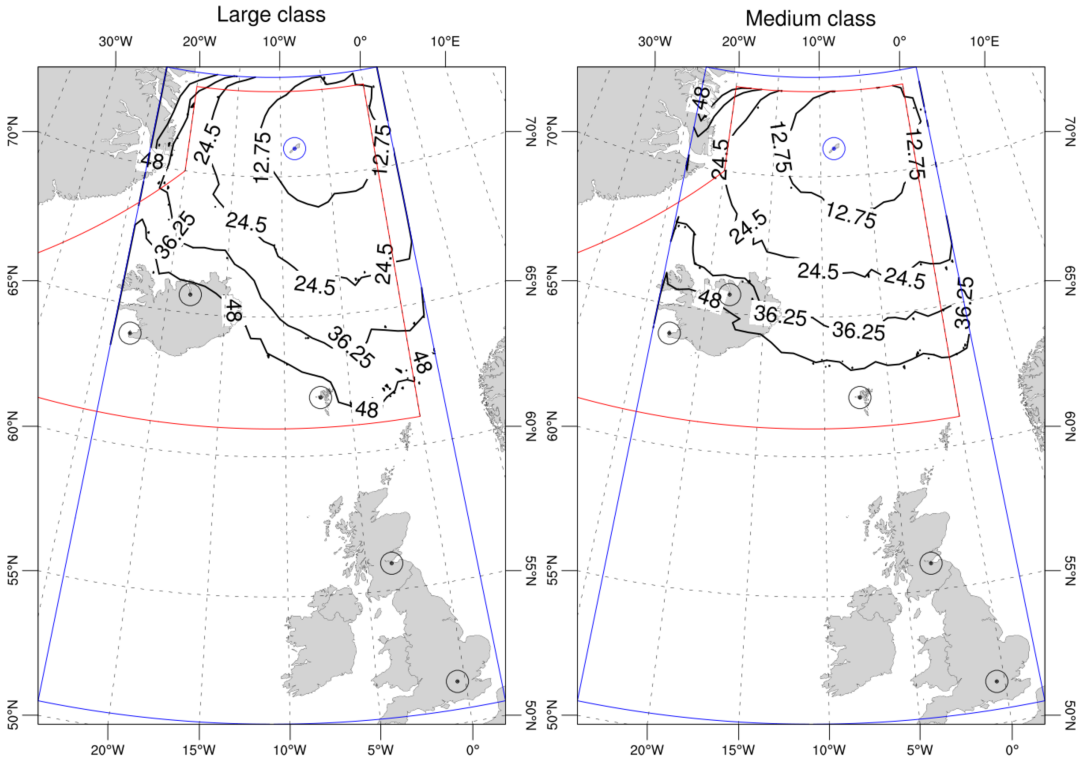


**Figure 8.** The Isolines show the arrival time in hours required for the ash concentration (at FL050) to exceed a threshold of 2 mg/m$^3$ with an exceedance probability of 5% between 0 and 48 hours after eruption. Black circles correspond to Keflavik and Akureyri (Iceland), Vágar (Faroe Islands), Edinburgh (Scotland) and Heathrow (U.K., London) airports.

Kristiansen et al. (2012) concluded that the main source of epistemic/aleatory uncertainty in ash dispersal forecasts comes from the quantification of the eruption source term (eruption column height and emission rate). Here, we address the quantification of uncertainty over the airborne tephra concentration and its extent. To do that, we assess the 95% confidence interval (i.e., range between the 97.5 and 2.5 percentiles) in the probability distributions describing the hazard curves for the concentration of tephra for each point in the domain. These probability distributions are deeply related to the number of simulations or scenarios used that model such concentrations, a detailed analysis of how the number of simulations affects the sensitivity of this uncertainty can be found in the Appendix A.

Figure 10 shows different maps, at different levels of confidence, produced by cutting the point-wise hazard curves at different percentiles. They correspond to a 4D analysis where concentrations are the highest at any time from the onset of the eruption up to 48 hours after its end.

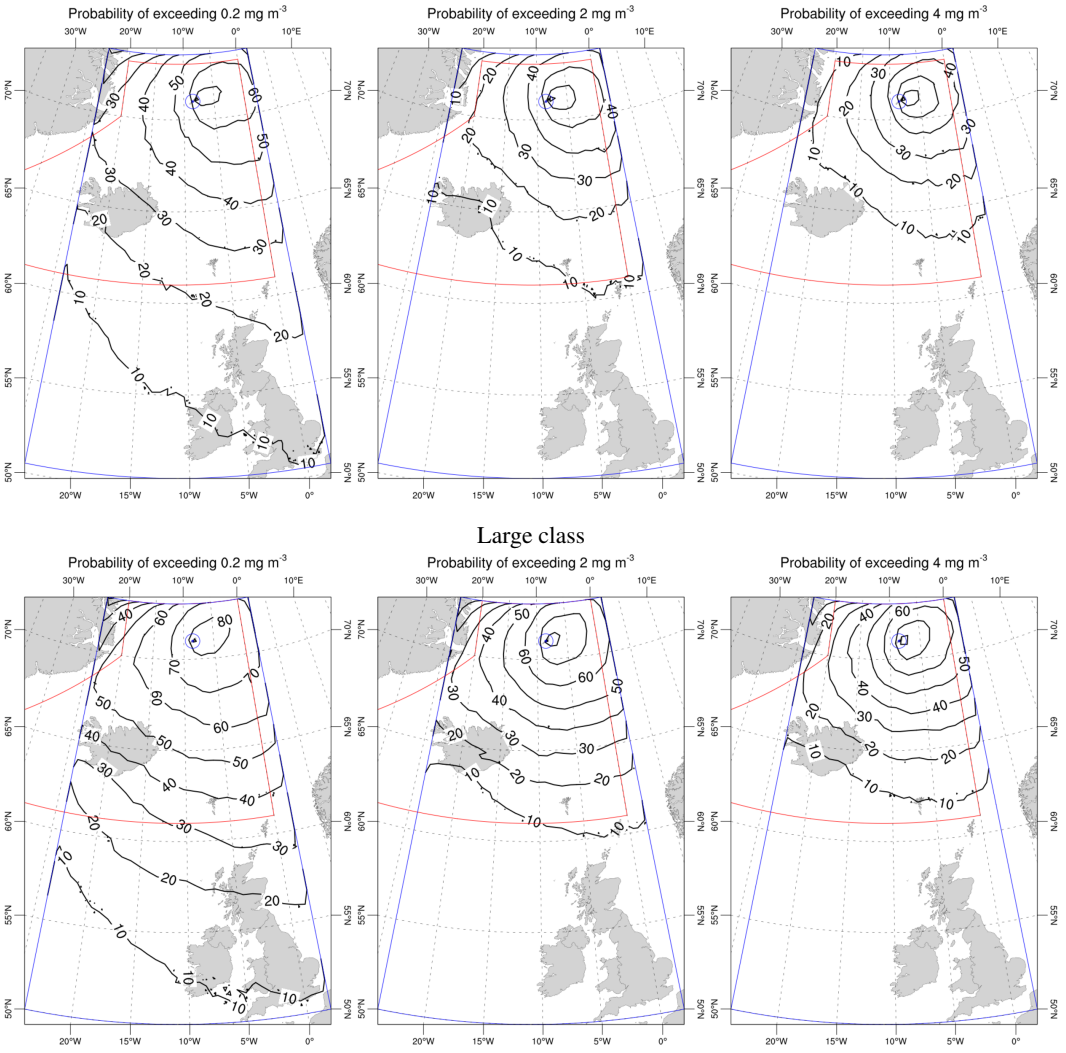


**Figure 9.** Exceedance probability maps at FL050: the isolines show the probability of reaching ash concentration above 0.2 mg/m$^3$ (left), 2 mg/m$^3$ (center) and 4 mg/m$^3$ (right) at FL050 at some time from the onset of the eruption up to 48 hours after its end. The three upper plots apply to the Large class and the three at the bottom to the Medium one.

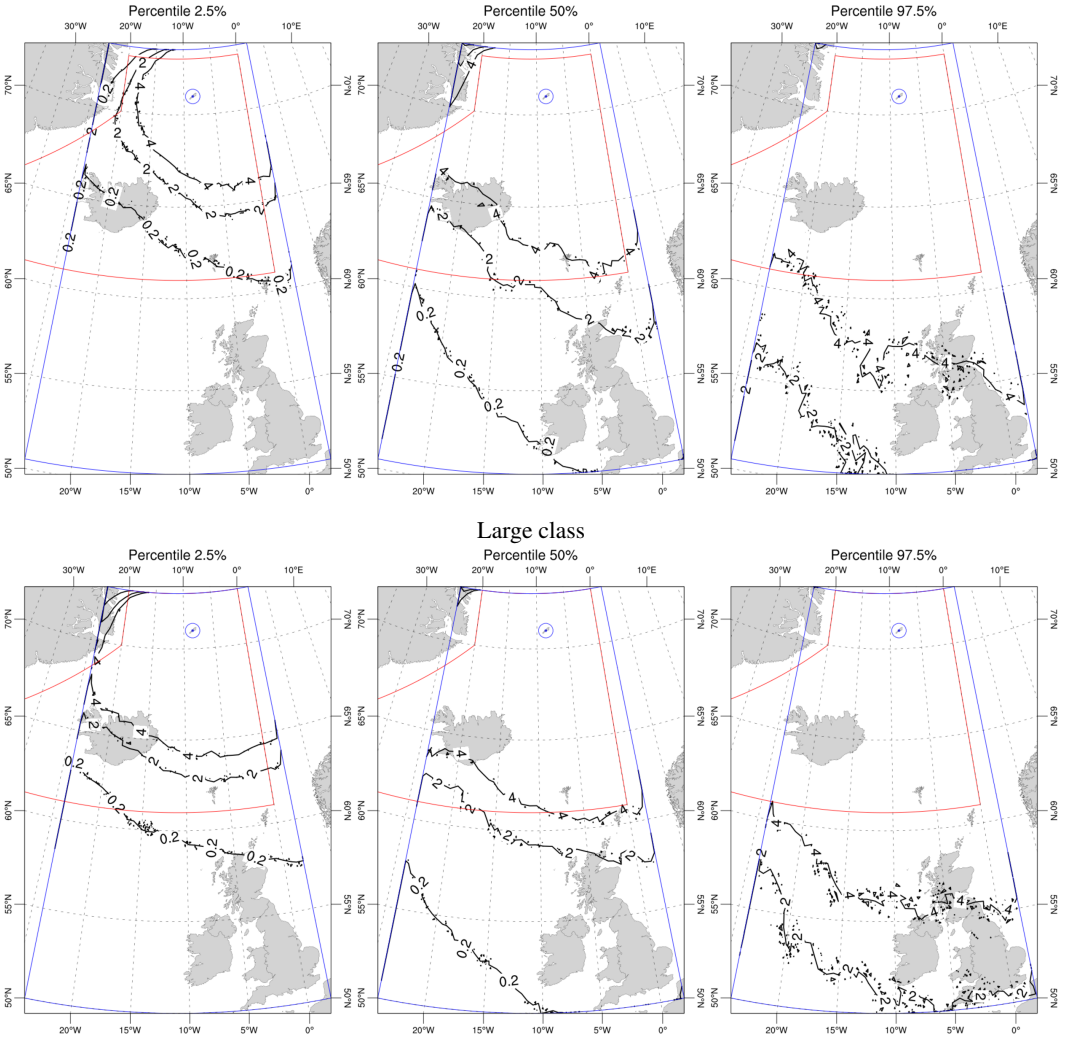


**Figure 10.** Concentration extent hazard map at FL050: relative uncertainties related with airborne ash cloud concentrations above 0.2 mg/m$^3$, 2 mg/m$^3$ and 4 mg/m$^3$ and extent. Each map corresponds to a different level of confidence, produced by cutting the point-wise hazard curves at different percentiles.

Figure 11 shows, from top-left to bottom-right, the probability of reaching or exceeding ash concentration above 2 mg/m$^3$ at FL050 for more than 1, 3, 6, 12, 18 and 24 hours, respectively, from the onset of a Large eruption up to 48 hours after its end. Figure 12 shows the same but for the Medium-size-eruption and, in the appendix, Figures D2 and D3 display the same information as Figures 11 and 12 but for FL250.

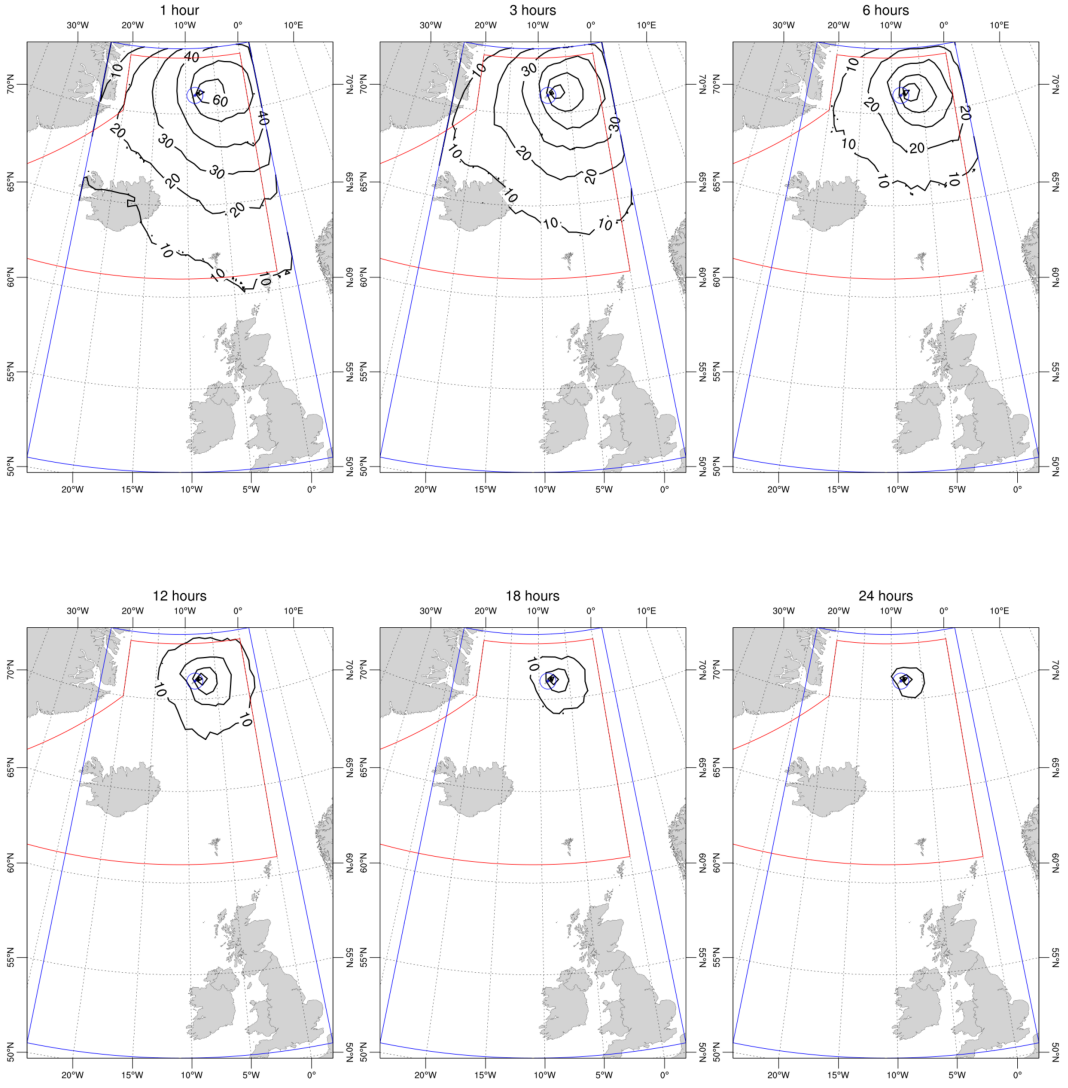


**Figure 11.** Persistence maps at FL050 (Large class): the isolines show probability of reaching or exceeding ash concentration above 2 mg/m$^3$ at FL050 1 hour, 3 hours, 6 hours, 12 hours, 18 hours, 24 hours during the eruption up to 48 hours after its end.

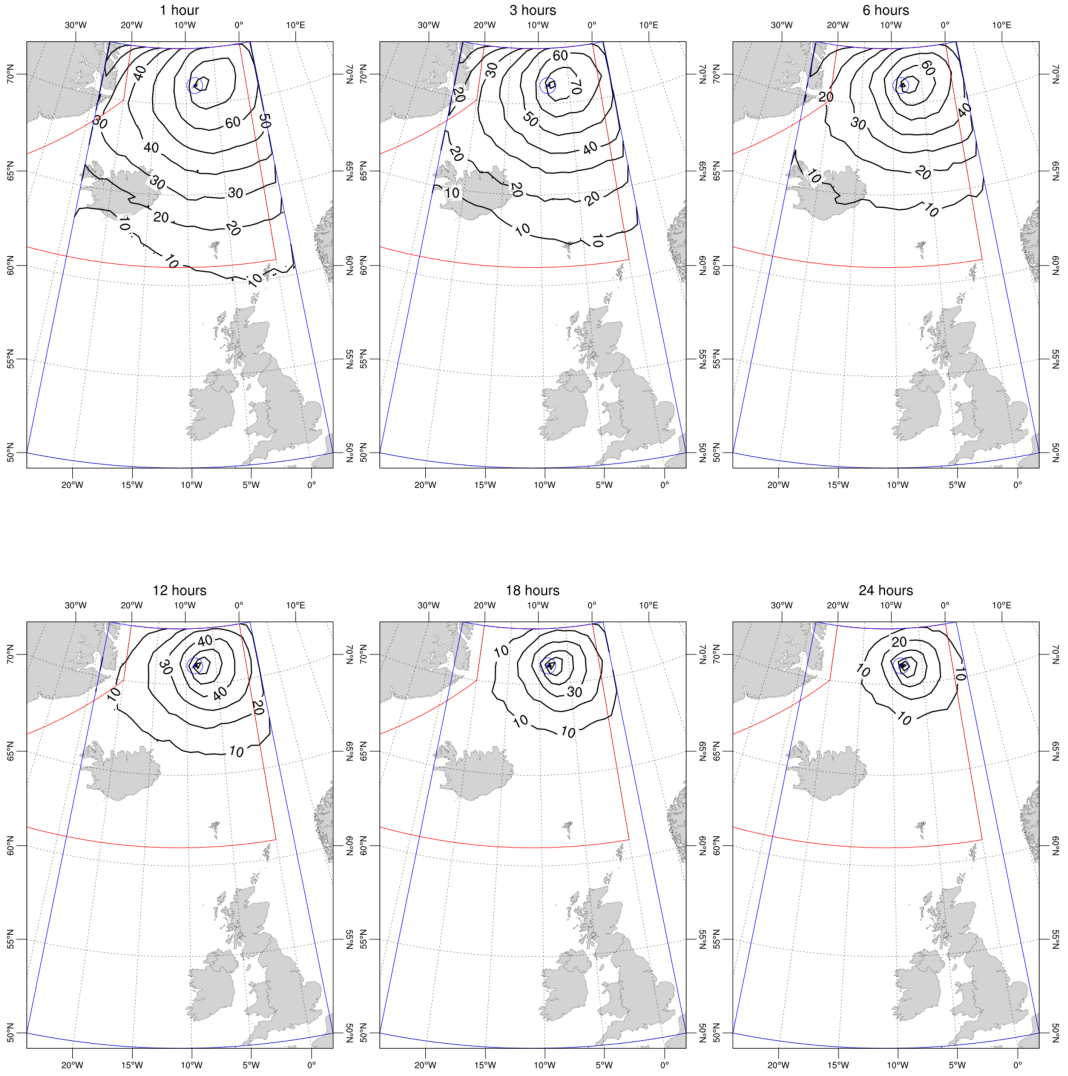


**Figure 12.** Persistence maps at FL050 (Medium class): the isolines show probability of reaching or exceeding ash concentration above 2 mg/m$^3$ at FL050 1 hour, 3 hours, 6 hours, 12 hours, 18 hours, 24 hours during the eruption up to 48 hours after its end.

**Table 2.** Airport locations, azimuth and distance to JM. Locations are expresed in Lat/Lon coordinates. Azimuth and distance correspond to azimut in degress and distance between JM Island and the different airports.

| | Location (Lat/Lon) | Azimuth (°) | Distance (km) |
|---|---|---|---|
| Akureyri (Iceland) | 65.658 N, 18.073 W | 218.25 | 712 |
| Keflavik (Iceland) | 63.986 N, 22.627 W | 224.50 | 981 |
| Vágar (Faroe Island) | 62.063 N, 7.277 W | 176.51 | 994 |
| Edinburgh (Scotland) | 55.948 N, 3.363 W | 169.11 | 1690 |
| Heathrow (England) | 51.472 N, 0.454 W | 165.25 | 2208 |

## 5 Discussion

Results have been carried out considering the intrinsic limitations of the methodology (partially due to the scarcity of data related with complete geological record composed of both chronological and statistical data). This fact is important, as future advances in the geological cataloge could have implications on future work assessing volcanic hazards and mitigating measures on JM.

### 5.1 Arrival time maps

As shown in Figure 8, an ash-rich eruption originating from JM volcano has potential to affect the air traffic over Iceland after 36 hours and, to some extent, the Faroe Island or archipelago after 48 hours since the beginning of the eruption, with an exceedance probability of 5%.

Figure 13 shows the evolution of the probability over time of ash concentration exceeding 2 mg/m$^3$ at FL050 and at international airports of Keflavik and Akureyri (Iceland), Vágar (Faroe Islands) and Heathrow (U.K., London) (see Table 2 for distance references). The probability at any airport is neglectable during the first hours (approx. 10 and 15 hours for Medium and Large classes respectively) and then increases until stabilizing after several days (approx. 7 and 5 days for Medium and Large classes respectively). For both eruption classes, Vágar airport has a higher probability of exceeding such threshold than other nearest airports as Keflavik. This is due to a very marked difference in the wind patterns between the North-NorthEast and the West. After 48 hours since the beginning of the eruption, only Akureyri airport should exceed probabilities above 5% to reach the concentration threshold of 2 mg/m$^3$ for a Medium class eruption. No airport shows exceedance probabilities for such critical threshold above 25%.

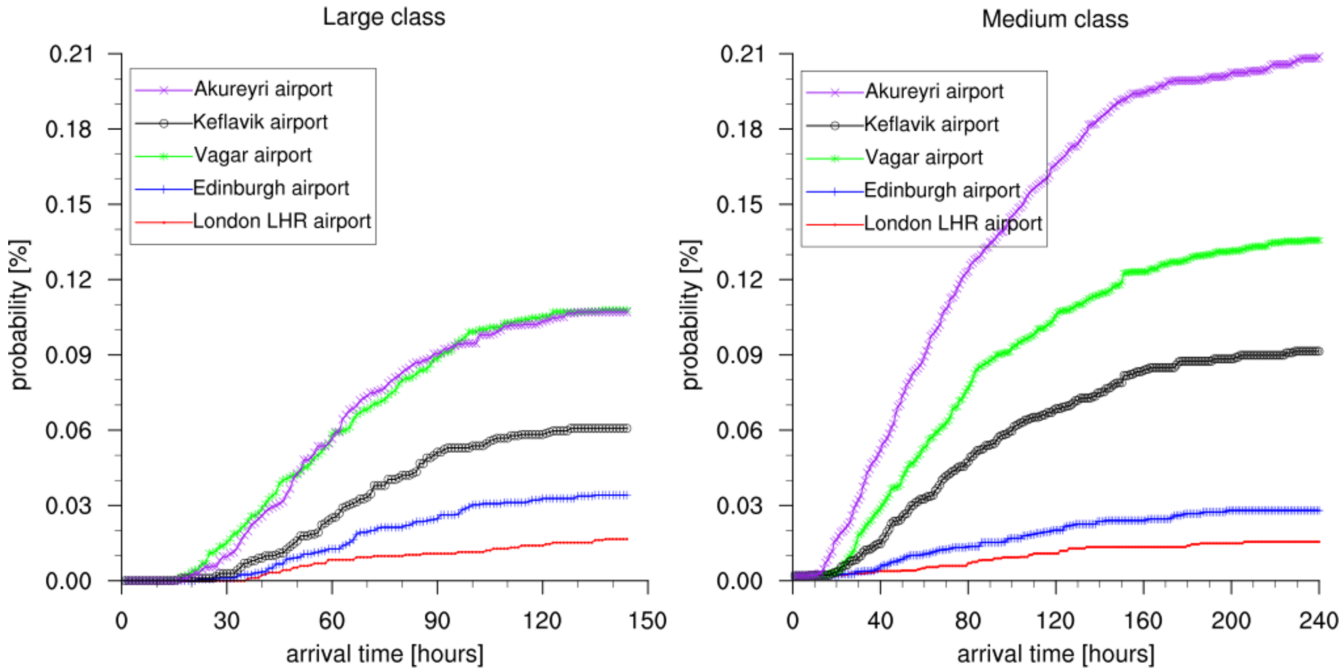


**Figure 13.** Exceedance probabilities vs arrival times required for the ash concentration (at FL050) to exceed a threshold of 2 mg/m$^3$ at different airports for Medium and Large eruptions since the beginning of the eruption.

## 5.2 Exceedance probability maps

Figures 9 and D1 in the Appendix D show substantially different results regarding ash concentration and extent for both eruption classes. Regarding concentrations, for Large class, values above 2 mg/m$^3$ (reaching even 4 mg/m$^3$, originally considered no fly zone) would affect part of the Icelandic FIR with exceedance probabilities between 10 and 50%. Instead, for Medium class, such concentrations would affect only low flight levels. Above FL250, moderate-higher probabilities are only found in polar routes. This is due to the fact that the height of the eruptive column for Medium magnitude class eruptions does not exceed 11 km (see Section 3.1). These results are in agreement with those shown in Figure 10 (where maps, at different levels of confidence, were produced by cutting the hazard curves at distinct percentiles to depict the relative uncertainties related with airborne ash cloud concentrations and extent for both eruption classes at FL050).

Concerning the extent, at FL050, ash concentrations up to 2 mg/m$^3$ could reach almost the entire Icelandic FIR with probabilities between 10-50% for both eruption classes. It could threaten the vast majority of flights to and from northern routes. Instead, at FL250, ash clouds would affect the North-East of Iceland for concentrations up to 0.2 mg/m$^3$ only when Large size eruption occurs. Then, we can conclude that for Medium class, only polar routes above FL250 would be threatened.

Finally, in a similar way to other types of analysis such as tephra ground load and Probabilistic Seismic Hazard Assessment, Figure 14 provides a graphical representation of relative uncertainties related with airborne ash cloud concentrations above 0.2

mg/m$^3$, 2 mg/m$^3$, and 4 mg/m$^3$ at FL050 at Keflavik airport. This result, computed at each point of the target domain, could be eventually used as input for risk analysis like for producing fragility curves, tolerance analysis and in general investigation of impact on infrastructure. In this view, it represents the most complete way to quantify hazard. Specifically, no dramatic differences are seen depending on the eruption size, and there is a non-negligible probability to overcome the 2 mg/m$^3$ threshold, even for low percentiles, given an eruption.

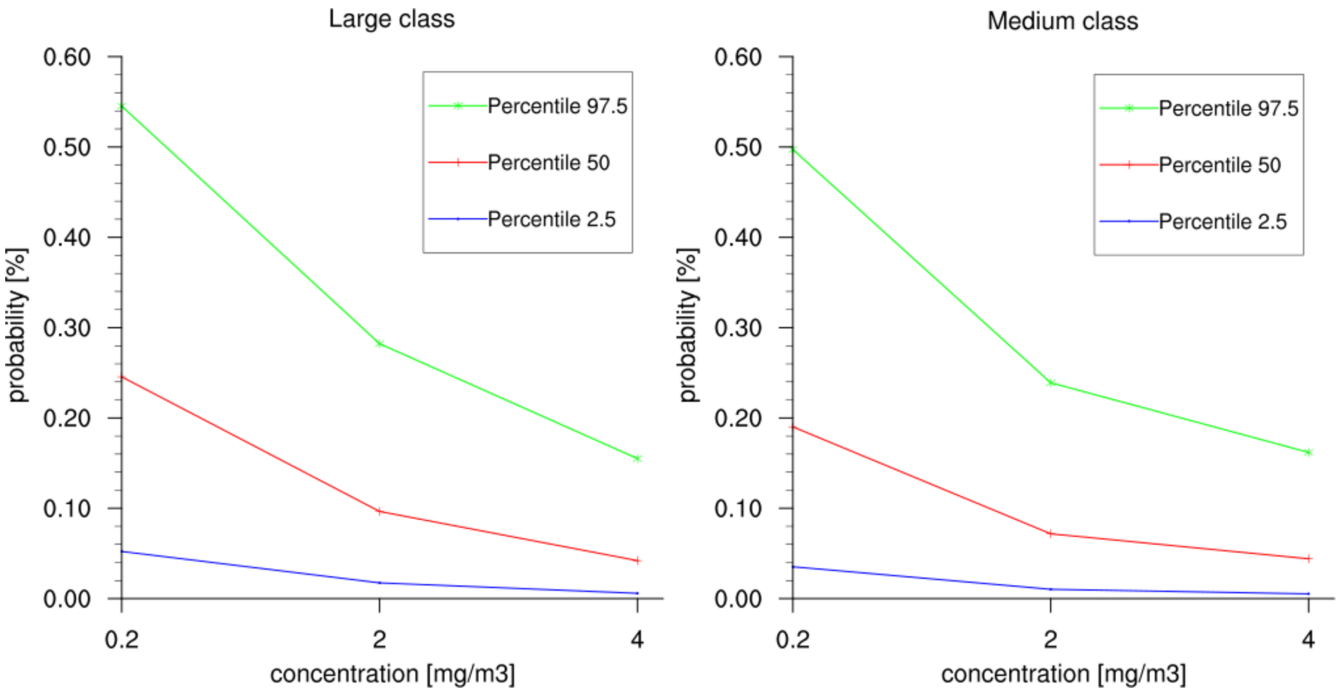


**Figure 14.** Concentration analysis: relative uncertainties related with airborne ash cloud concentrations above 0.2 mg/m$^3$, 2 mg/m$^3$ and 4 mg/m$^3$ at FL050 at Keflavik airport.

### 5.3 Persistence maps

According to Figure 7, jet engines exposed to concentration conditions of up to 4 mg/m$^3$ for more than 3 hours would require inspection. This motivates the spatio-temporal analysis of persistent high concentration scenarios. In terms of ash cloud extent, results (Figures 11 and 12) are slightly different: at FL050 a large part of Icelandic FIR (reaching in some extent Faroe island) with probabilities between 10 and 50% would be affected for both eruption classes up to a total of 6 hours since the eruption beginning. Instead, at FL250 (Figures D2 and D3)), such conditions would affect only high latitude air routes (above 68° N). For high concentration scenarios longer than 12 hours, some differences between the eruption class can be observed. At FL050, an ash cloud has probabilities lower than 10% to reach latitudes as low as 68° N and 66° N for Large and Medium eruption

respectively. Such southernmost latitude increases for longer persistence values, meaning that (obviously) only closer to the source we may get long-persisting clouds.

Finally, Figure 15 presents a persistence analysis for the airports considered in this study, showing the exceedance probability of reaching ash concentration above the critical condition for maximum risk actions like takeoff or landing until 24 hours since the beginning of the eruption. The most affected airports are Akureyri, Vagar and Keflavik. London LHR has very low probabilities (1.5%-2%) associated to 1 to 6 hours persistence scenarios until 48 hours after the beginning of the eruption. Concerning the level of persistence, both eruption classes have similar behavior. Scenarios with persistence larger than 18 hours are highly unlikely. However, when analyzing probabilities, Medium class reachs values twice higher than Large one. This observation can again be associated with their eruptive dynamic. The sustained injection of tephra into the atmosphere related with a series of discrete short-lived events increases the probability of prolonged high concentration scenarios.

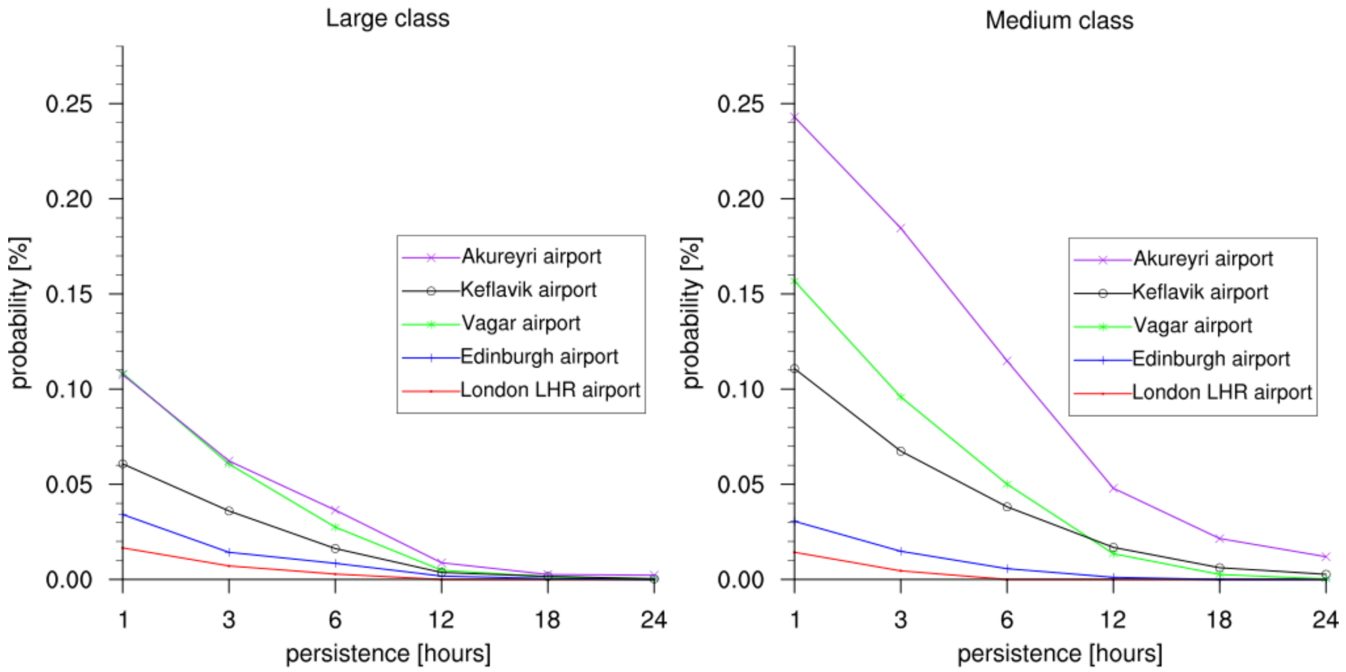


**Figure 15.** Persistence analysis for ash concentration up to 2 mg/m$^3$ at FL050. Exceedance probability of reaching or exceeding ash concentration above 2 mg/m$^3$ at FL050 1 hour, 3 hours, 6 hours, 12 hours, 18 hours, 24 hours at different airports during the eruption up to 48 hours after its end.

## 6 Conclusions

Despite the partial geological record can be a bias for hazard assessment for JM island, the spatio-temporal analysis presented here provides the first comprehensive analysis of potential impact on aviation safety in the North Atlantic due to a future explosive activity.

An ash-rich eruption originating from JM volcano has potential to affect air traffic over Iceland (after 36 hours) and, to some extent, the Faroe Island, after 48 hours. Concerning airborne ash concentration and extent, for Large eruptions, concentrations above 2 mg/m$^3$ (even 4 mg/m$^3$, originally considered no fly zone) would affect part of the Icelandic airspace (at different flight levels) with exceedance probabilities between 10 and 50% at some time from the onset of the eruption up to 48 hours after its end. For Medium eruptions, these dangerous concentrations would affect only low flight levels (FL050). Above FL250 only polar routes would be affected.

When analyzing persisting concentration conditions where aircraft engines are exposed to high concentration for more than 3 hours, we conclude that at FL050 a large part of icelandic FIR (reaching in some extent U.K.) with probabilities 5 and 50% would be affected for both Medium and Large eruption classes. At FL250 such risky conditions would affect only high latitude air routes (above 68° N).

Finally we want to highlight the robustness of our PVHA in terms of uncertainty quantification, that should be routinely considered in all this kind of studies.

*Code and data availability.* Scripts and pipeline programs will be uploaded according to the manuscript preparation guidelines

This section provides an overview about the High Performance Computing (HPC) environment used in this study and the setup process associated with the FALL3D model to simulate the eruptive scenarios. The most relevant settings to optimize the computational resources, as well as the simulation scheme followed are described.

## Appendix A: Simulation setup

To account for the meteorological statistics in the simulation results of each eruptive class (Large and Medium), 1500 wind fields over the time period 1999–2020 were randomly sampled from ECMWF ERA5 Reanalysis dataset. Then, 1500 simulations (scenarios) combining meteorological conditions and ESP for each class were run. Since Medium eruptive class is characterized by a series of discrete short-lived events, the total number of scenarios for such class was 3763. The total used CPU/GPU hours was 9.6M, considering the architectures showed in Table C1 in Appendix C.

Figure A1 shows the variance of the tephra concentration at a given grid-point with respect to the number of scenarios simulated. After 900 scenarios, the variance of the concentration begins to stabilize. This stabilization also suggests a reduction in uncertainty related to the intra-size variability of the eruptive scenarios themselves.

All the scenarios were ran using Fall3D-8.1 model (Folch et al., 2020) over a 2000 km $\times$ 2000 km domain between 50°N and 73°N (on latitude) and 2°W and 24°W (on longitude) with a resolution of about 2 km. Eruptive vents were placed at (70.98°N, 8.38°W) and (71.10°N ,8.13°W) respectively for Medium and Large eruptive classes.

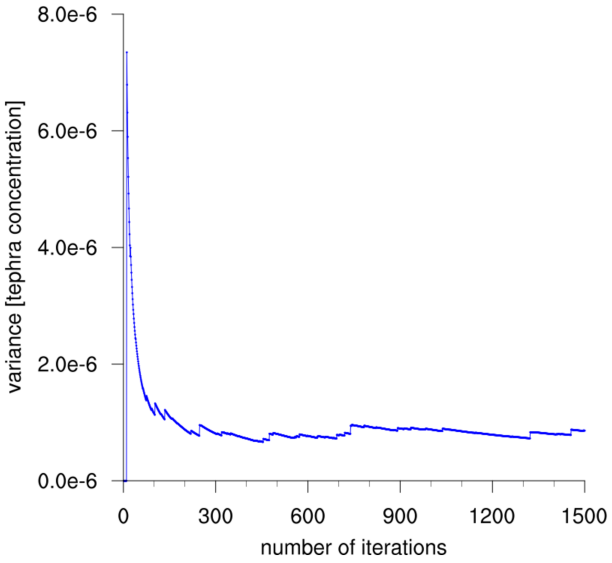


**Figure A1.** Value of the variance of tephra concentration for a given grid-point with respect to the number of scenarios simulated.

## Appendix B: Sampling and processing workflow

For each eruptive class, the PDFs describing each ESP were fixed following Sandri et al. (2016). It is important to note that this work only addressed the Medium and Large eruptive classes. Table B1 summarizes the PDFs and values ranges of the main ESP for JM island. The sampling process can be described as:

1. Sample a value for total erupted volume (or magnitude), duration of the fallout phase, column shape and sphericity of tephra particles from their PDFs. The total erupted volume, expressed as DRE is computed uniformly within a range of values ($10^{8}$ -$10^{8.9}$ $m^3$). In a second step, we weight each total eruption volume based on the Weibull distribution function previously defined (Figure 2). In this way the unlikely events are properly represented.

2. Compute the mass fraction (%) associated to tephra fallout with respect to the total erupted mass according to the available estimations from field data analysis. For Medium eruptive class, the value of % is fixed to 0.8, whereas for Large eruptive class is randomly sampled from [0.05, 0.10].

3. Compute the mass eruption rate and the column heights from total erupted volume sampled. The mass eruption rates ranges between 3.009x$10^{4}$ -1.5x$10^{6}$ kg/s and 6.94x$10^{4}$ -1.39x$10^{6}$ kg/s for Medium and Large eruptive sizes respectively.

**Table B1.** PDFs and values ranges of the main eruptive parameters for JM island. Bounds on Mass Eruption Rate values are a consequence of the sampling procedure for total erupted volume (Figure 3) and duration of the fallout phase described in the text. For the total grain size distribution, references were chosen from Eggoya 1732 and Grimsvönt 2004 eruptions for Medium and Large classes respectively. Erupted volumes are between 0.1–0.5, and $>$0.5 km$^3$ for Medium, and Large classes ranges.

| Parameter | Eruption Class | PDF type and ranges |
|---|---|---|
| Total erupted volume (Kg$^a$) | Medium | Weibull on [$10^8$;$10^{8.7}$] |
| | Large | Weibull on [$10^{8.7}$;$10^{8.9}$] |
| Duration of fallout (hours) | Medium | Uniform on [96;960] composed by pulses |
| | Large | Uniform on [24;120] |
| Mass eruption rate (kg/s) | Medium | [3.009*$10^4$;1.5*$10^6$] |
| | Large | [6.94x$10^4$;1.39x$10^6$] |
| Total Grain Distribution modes (Φ- units) | Medium | Eggoya 1732 Surtseyan eruption reference |
| | Large | Grimsvötn 2004 eruption reference |
| Density of tephra particles (kg/m$^3$) | Medium | 1300 |
| | Large | 1200 |
| Tephra mass fraction (%) | Medium | 80 |
| | Large | Uniform on [5;10] |
| Density of particles aggregates (kg/m$^3$) | both types | Aggregate 1: 250 |
| | | Aggregate 2: 350 |
| Diameter of particles aggregates (Φ- units) | both types | Aggregate 1: 100 |
| | | Aggregate 2: 250 |

The source term (vertical distribution of mass in the eruption column) is given by a Suzuki distribution (Suzuki et al., 1983) with the parameter A in the range 3 to 4.5 and $\lambda = 1$.

4. Sample a time for the eruption start over a period of 21 years (1999–2020) considering the corresponding meteorological fields for the duration of the fallout phase, and associate this randomly to a combination of the volcanological parameters. For this, ECMWF ERA5 reanalysis meteorological data have been used associated with the date and duration of the eruption. Modify FALL3D's input file with both, meteo and newly sampled data values.

5. Run FALL3D to obtain the tephra loading at different flight levels. Ganser terminal velocity model (Ganser, 1993) and the CMAQ model parameterization for horizontal diffusion (Folch et al., 2009) were used as part of model physics configuration.

6. The outputs obtained from FALL3d are computed. As a result, hazard and probabilistic maps describing the airborne ash concentration and time-persistence at different flight levels on a large-scale and high-resolution domain are obtained.

Typical tephra particle densities and total grain size distributions were chosen consistent with previous values reported for Eggoya (1790) and Grimsvötn (2004) eruptions for Medium and Large classes respectively. The type of aggregates were also chosen consistent with previous values reported for similar Surtseyan and phreatomagmatic eruptions.

## Appendix C: Computational resource

Experiments were run on Joliot-Curie, at Très Grand Centre de calcul du CEA (The French Alternative Energies and Atomic Energy Commission (CEA) /TGCC).

Considering that FALL3D-8.1 uses MPI for 3D domain decomposition with freedom for the user to choose the number of processors along each spatial direction, to identify the optimal running configuration on Irene-rome and Irene-skylake, a few benchmark cases (with grid size similar to that of the real benchmark ones, 50M grid points and 12 particle bins) were ran changing the configuration of nodes and cores used. Results are shown in Figure C1.

**Table C1.** Joliot- Curie supercomputer. Characteristics corresponding with the two partitions available on this study.

| Machine | Institution | Hardware |
|---|---|---|
| Irene-Rome | CEA/TGCC | 2292 AMD Rome 2.6GHz bi-processor compute nodes with 128 cores per node (64x2).This totals 293376 compute cores and 11.75 PFlop/s peak power. |
| Irene-Skylake | CEA/TGCC | 1656 Intel-skylake 2.7GHz bi-processor compute nodes with 48 cores per node (24x2).This totals 79488 cores with 180GBy/node. |

As observed, for this particular grid size, parallel efficiencies are substantially better at Irene-rome, with >90% up to 2048 processors (16 nodes). At the Irene-skylake partition, parallel efficiencies already drop to 70% with only 1036 processors

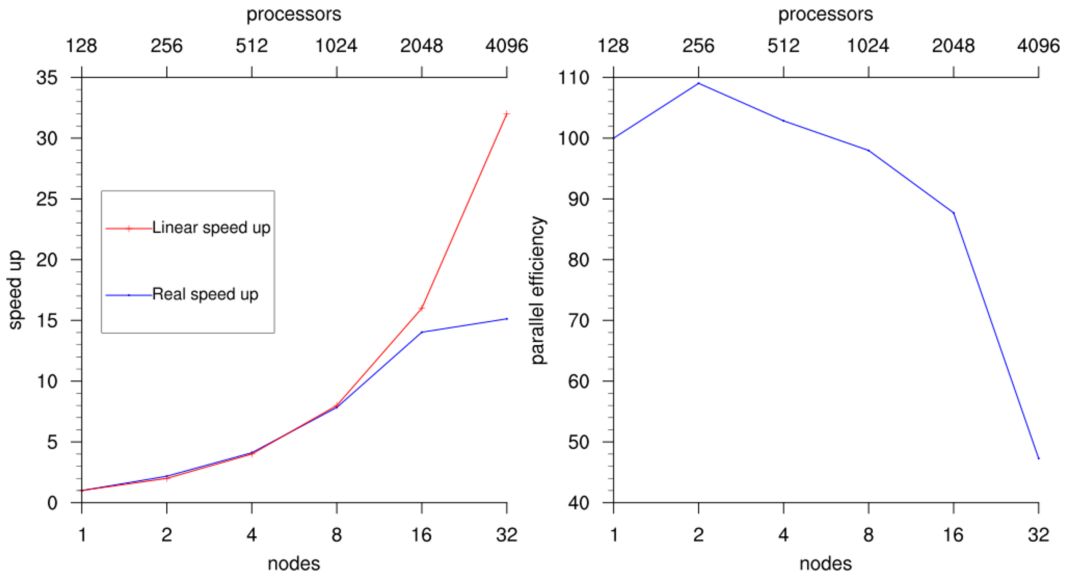


Irene Rome

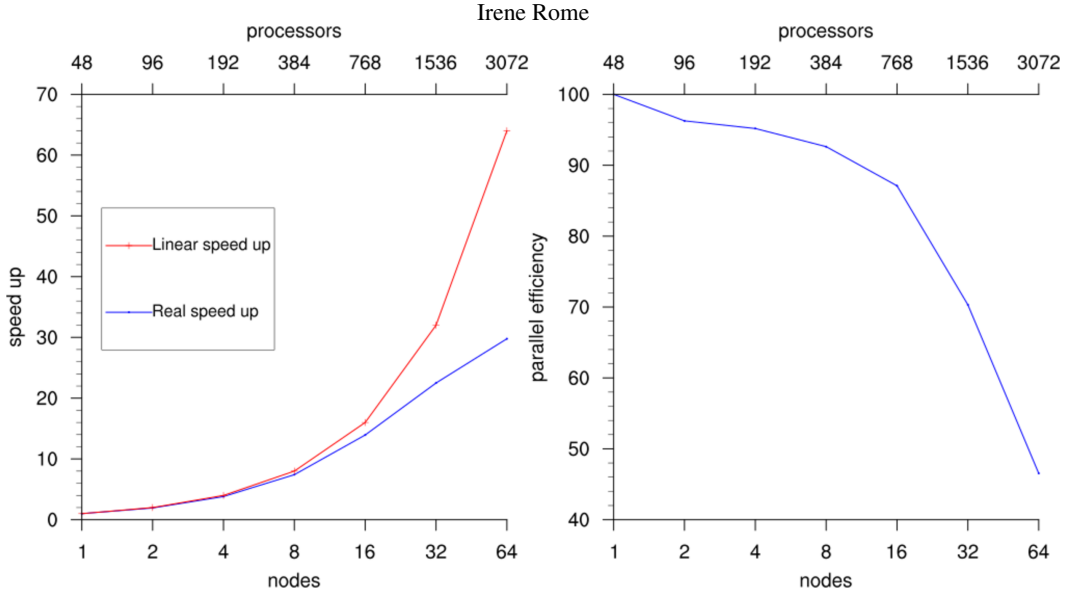


Irene Skylake

**Figure C1.** Strong scalability analysis (time to solution). Top: speed-up and parallel efficiency analysis at Irene-rome (128 AMD processors per node). Bottom: same for Irene-skylake (48 skylake processors per node).

(32 nodes). Scalability breaking at a larger number of processors occurs because the number of grid points per sub-domain becomes less than the specific range in which communications start to overtake computations (a larger grid size would be needed to sustain speed-up ratios close to optimal above 2048 processors). Then, considering the resolution of our domain (0.025º), and the total grid points 35M (1040x920x35x14), we fixed the number of nodes to 16 and the number of cores to 768. This configuration allows decomposing the grid points into 32x24x1 (X, Y, Z) subdomains of more than 30 points per spatial dimension. As a result, we increased the speed-up 16 times and the parallel efficiency was fixed to 90%.

## Appendix D: Complementary maps

### D1 Exceedance probability maps at FL250

Figure D1 shows the exceedance probability maps computed at FL250.

### D2 Persistence maps at FL250

Figures D2 and D3 show the exceedance probability maps computed at FL250.

*Author contributions.* Sara Barsotti, Laura Sandri, Arnau Folch, Giovanni Macedonio, and Antonio Costa contributed to the conception and design of study, analysis and/or interpretation of data and drafting the manuscript. Manuel Titos, Beatriz Martinez Montesinos and Leonardo Mingari contributed to coding the scripts and software, analysis and/or interpretation of data and drafting the manuscript.

*Competing interests.* The authors declare that author Giovanni Macedonio is a member of the editorial board of the journal.

*Acknowledgements.* The research leading to these results has received funding from the European Union's Horizon 2020 research and innovation programme under the ChEESE project, grant agreement N° 823844.We thank the multi-year PRACE Project Access "Volcanic Ash Hazard and Forecast" (ID 2019215114).

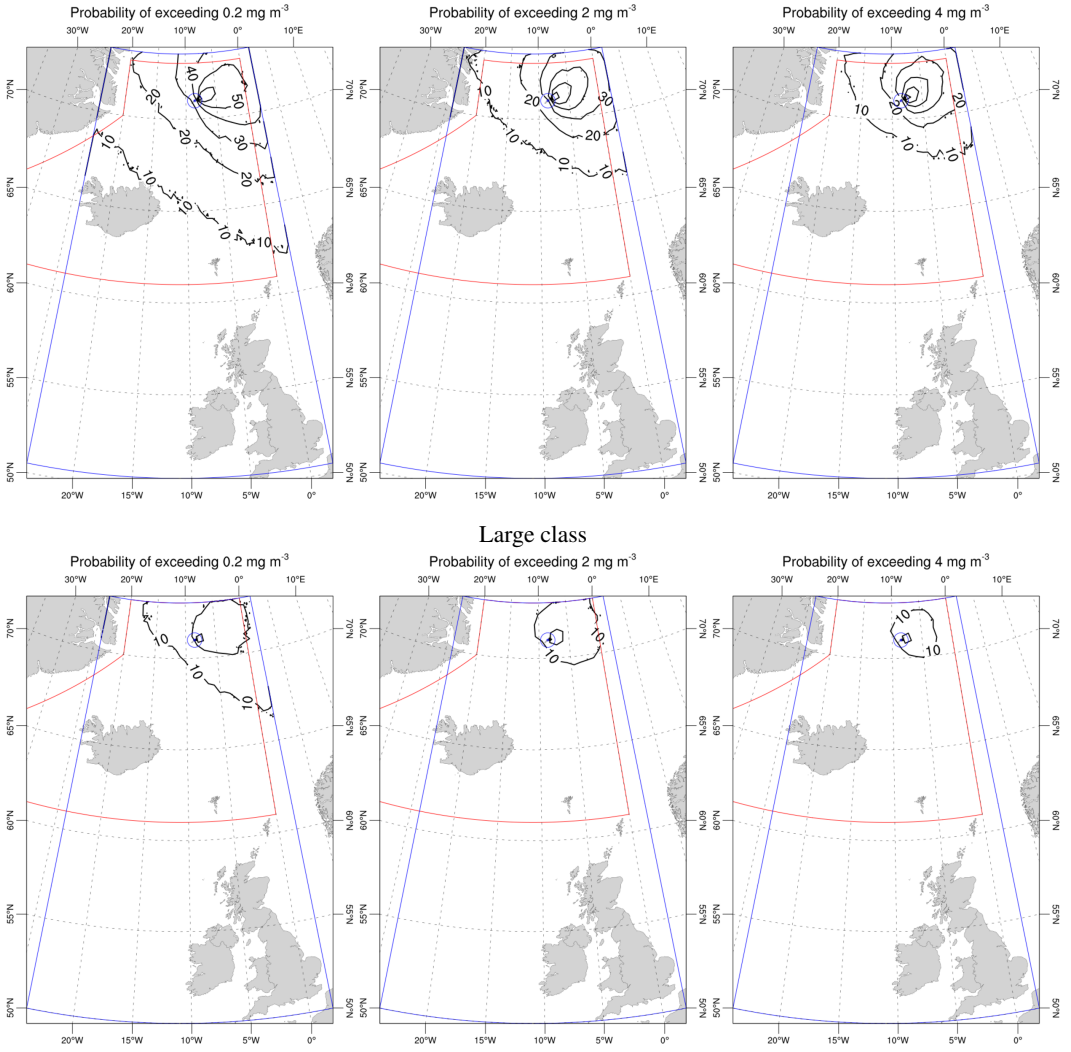


**Figure D1.** Exceedance probability maps at FL250: the isolines show the probability of reaching ash concentration above 0.2 mg/m$^3$ (left), 2 mg/m$^3$ (center) and 4 mg/m$^3$ (right) at FL250 at some time from the onset of the eruption up to 48 hours after its end.

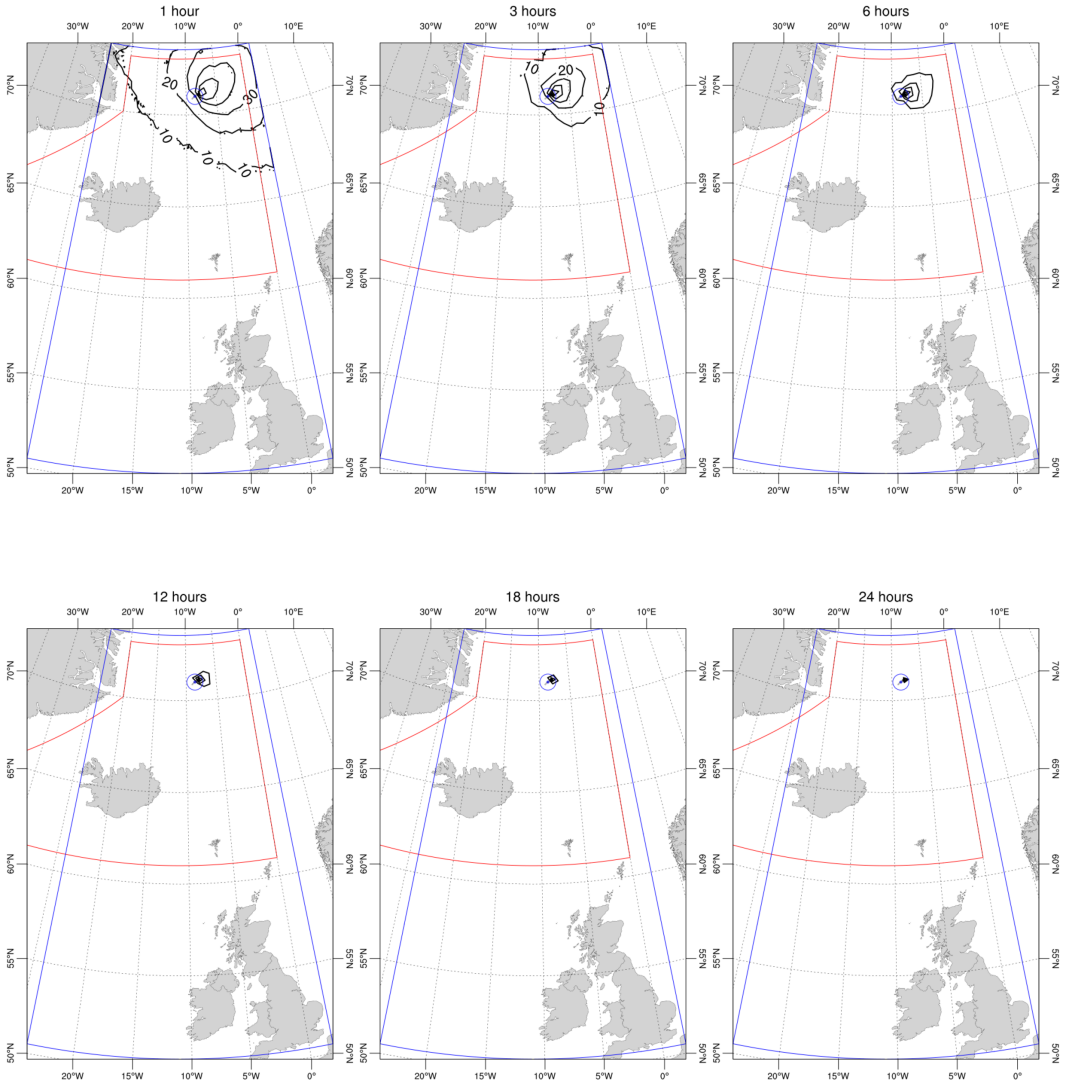


**Figure D2.** Persistence maps at FL250 (Large class): the isolines show probability of reaching or exceeding ash concentration above 2 mg/m$^3$ at FL250 1 hour, 3 hours, 6 hours, 12 hours, 18 hours, 24 hours during the eruption up to 48 hours after its end.

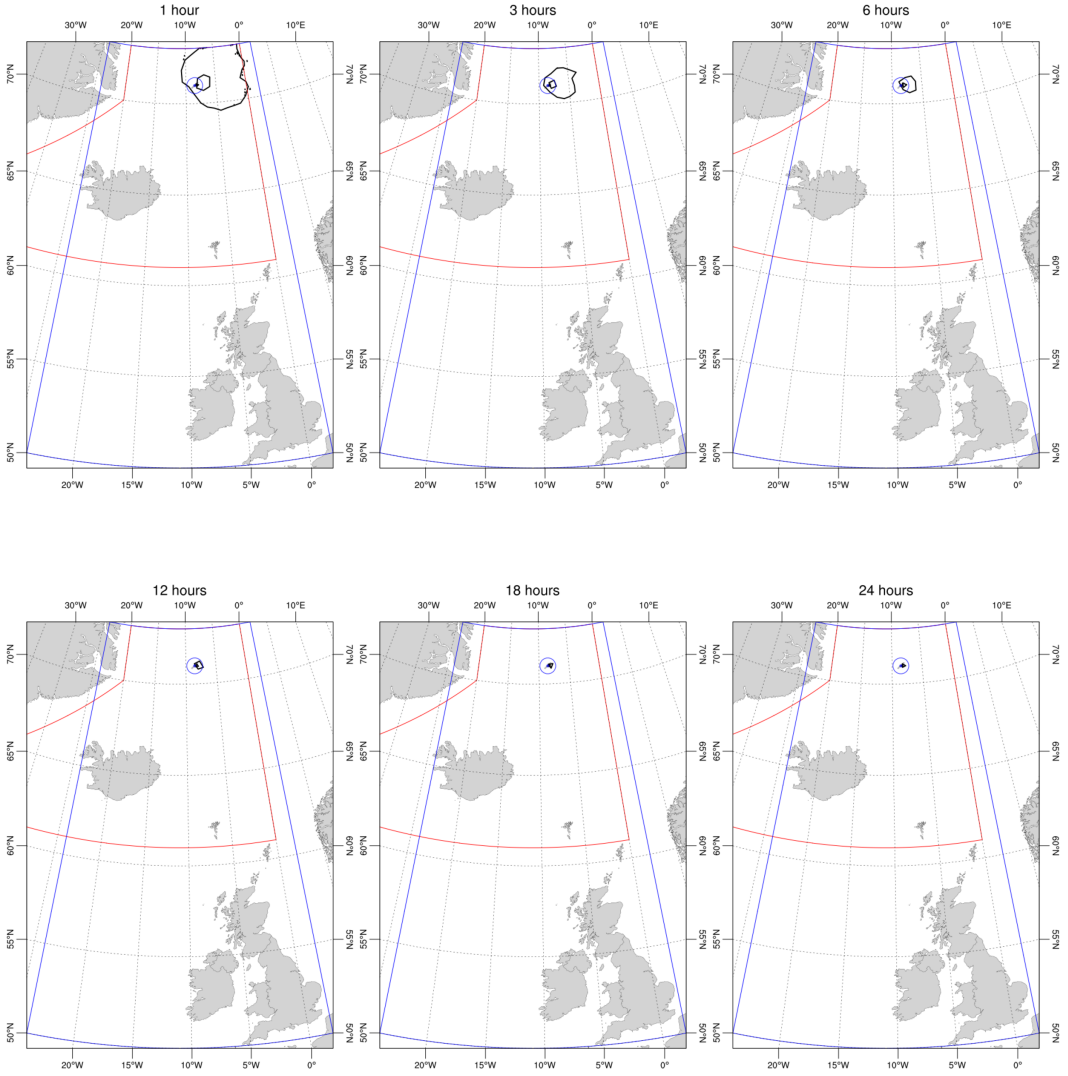


**Figure D3.** Persistence maps at FL250 (Medium class): the isolines show probability of reaching or exceeding ash concentration above 2 mg/m$^3$ at FL250 1 hour, 3 hours, 6 hours, 12 hours, 18 hours, 24 hours during the eruption up to 48 hours after its end.

## References


Abbott, P. M. and Davies, S. M.: Volcanism and the Greenland ice-cores: the tephra record, Earth-Science Reviews, 115, 173–191, 2012.

Akaike, H.: Information theory and an extension of the maximum likelihood principle, in: Selected papers of hirotugu akaike, pp. 199–213, Springer, 1998.

Amante, C. and Eakins, B. W.: ETOPO1 arc-minute global relief model: procedures, data sources and analysis, 2009.

Barsotti, S., Di Rienzo, D. I., Thordarson, T., Björnsson, B. B., and Karlsdóttir, S.: Assessing impact to infrastructures due to tephra fallout from Öræfajökull volcano (Iceland) by using a scenario-based approach and a numerical model, Frontiers in Earth Science, 6, 196, 2018.

Blischke, A., Gaina, C., Hopper, J., Péron-Pinvidic, G., Brandsdóttir, B., Guarnieri, P., Erlendsson, Ö., and Gunnarsson, K.: The Jan Mayen microcontinent: an update of its architecture, structural development and role during the transition from the Ægir Ridge to the mid-oceanic Kolbeinsey Ridge, Geological Society, London, Special Publications, 447, 299–337, 2017.

Bonadonna, C., Connor, C. B., Houghton, B., Connor, L., Byrne, M., Laing, A., and Hincks, T.: Probabilistic modeling of tephra dispersal: Hazard assessment of a multiphase rhyolitic eruption at Tarawera, New Zealand, Journal of Geophysical Research: Solid Earth, 110, 2005.

Bozdogan, H.: Model selection and Akaike's information criterion (AIC): The general theory and its analytical extensions, Psychometrika, 52, 345–370, 1987.

Brendryen, J., Haflidason, H., and Sejrup, H. P.: Norwegian Sea tephrostratigraphy of marine isotope stages 4 and 5: prospects and problems for tephrochronology in the North Atlantic region, Quaternary Science Reviews, 29, 847–864, 2010.

Budd, L., Griggs, S., Howarth, D., and Ison, S.: A fiasco of volcanic proportions? Eyjafjallajökull and the closure of European airspace, Mobilities, 6, 31–40, 2011.

Budnitz, R., Apostolakis, G., and Boore, D. M.: Recommendations for probabilistic seismic hazard analysis: guidance on uncertainty and use of experts, Tech. rep., Nuclear Regulatory Commission, Washington, DC (United States). Div. of Engineering Technology; Lawrence Livermore National Lab., CA (United States); Electric Power Research Inst., Palo Alto, CA (United States); USDOE, Washington, DC (United States), 1997, 1997.

Clarkson, R. J., Majewicz, E. J., and Mack, P.: A re-evaluation of the 2010 quantitative understanding of the effects volcanic ash has on gas turbine engines, Proceedings of the Institution of Mechanical Engineers, Part G: Journal of Aerospace Engineering, 230, 2274–2291, 2016.

Elefante, L., Jalayer, F., Iervolino, I., and Manfredi, G.: Disaggregation-based response weighting scheme for seismic risk assessment of structures, Soil Dynamics and Earthquake Engineering, 30, 1513–1527, 2010.

Elissondo, M., Baumann, V., Bonadonna, C., Pistolesi, M., Cioni, R., Bertagnini, A., Biass, S., Herrero, J.-C., and Gonzalez, R.: Chronology and impact of the 2011 Cordón Caulle eruption, Chile, Natural Hazards and Earth System Sciences, 16, 675–704, 2016.

Ellis, M., Bojdo, N., Filippone, A., and Clarkson, R.: Monte Carlo Predictions of Aero-Engine Performance Degradation Due to Particle Ingestion, Aerospace, 8, 146, 2021.

Folch, A. and Sulpizio, R.: Evaluating long-range volcanic ash hazard using supercomputing facilities: application to Somma-Vesuvius (Italy), and consequences for civil aviation over the Central Mediterranean Area, Bulletin of Volcanology, 72, 1039–1059, 2010.

Folch, A., Costa, A., and Macedonio, G.: FALL3D: A computational model for transport and deposition of volcanic ash, Computers & Geosciences, 35, 1334–1342, 2009.

Folch, A., Mingari, L., Gutierrez, N., Hanzich, M., Macedonio, G., and Costa, A.: FALL3D-8.0: a computational model for atmospheric transport and deposition of particles, aerosols and radionuclides–Part 1: Model physics and numerics, Geoscientific Model Development, 13, 1431–1458, 2020.

Ganser, G. H.: A rational approach to drag prediction of spherical and nonspherical particles, Powder technology, 77, 143–152, 1993.

Gernigon, L., Blischke, A., Nasuti, A., and Sand, M.: Conjugate volcanic rifted margins, seafloor spreading, and microcontinent: Insights from new high-resolution aeromagnetic surveys in the Norway Basin, Tectonics, 34, 907–933, 2015.

Gjerløw, E., Höskuldsson, A., and Pedersen, R.-B.: The 1732 Surtseyan eruption of Eggøya, Jan Mayen, North Atlantic: deposits, distribution, chemistry and chronology, Bulletin of Volcanology, 77, 1–21, 2015.

Gjerløw, E., Haflidason, H., and Pedersen, R.: Holocene explosive volcanism of the Jan Mayen (island) volcanic province, North-Atlantic, Journal of Volcanology and Geothermal Research, 321, 31–43, 2016.

Harvey, N. J., Huntley, N., Dacre, H. F., Goldstein, M., Thomson, D., and Webster, H.: Multi-level emulation of a volcanic ash transport and dispersion model to quantify sensitivity to uncertain parameters, Natural hazards and earth system sciences, 18, 41–63, 2018.

Hill, L., Sparks, R., and Rougier, J.: Risk assessment and uncertainty in natural hazards, Risk and uncertainty assessment for natural hazards, edited by: Rougier, JC, Sparks, RS J., and Hill, LJ, pp. 1–18, 2013.

Hunt, J. B.: Tephrostratigraphical evidence for the timing of Pleistocene explosive volcanism at Jan Mayen, Journal of Quaternary Science, 19, 121–136, 2004.

ICAO: VOLCANIC ASH CONTINGENCY PLAN-EUROPEAN AND NORTH ATLANTIC REGIONS, https://www.icao.int/EURNAT/EUR%20and%20NAT%20Documents/EUR+NAT%20VACP%20v2.0.1-Corrigendum.pdf, 2021.

Imsland, P.: The geology of the volcanic island Jan Mayen, Arctic Ocean, Nordic Volcanological Institute, 1978.

Isavia: :annual report, https://www.isavia.is/annualreport2019/economy/flight-statistics, 2019.

Jakobsson, M., Mayer, L., Coakley, B., Dowdeswell, J. A., Forbes, S., Fridman, B., Hodnesdal, H., Noormets, R., Pedersen, R., Rebesco, M., et al.: The international bathymetric chart of the Arctic Ocean (IBCAO) version 3.0, Geophysical Research Letters, 39, 2012.

Kandilarov, A., Mjelde, R., Pedersen, R.-B., Hellevang, B., Papenberg, C., Petersen, C.-J., Planert, L., and Flueh, E.: The northern boundary of the Jan Mayen microcontinent, North Atlantic determined from ocean bottom seismic, multichannel seismic, and gravity data, Marine Geophysical Research, 33, 55–76, 2012.

Karlsdóttir, S., Gylfason, Á. G., Höskuldsson, Á., Brandsdóttir, B., Ilyinskaya, E., Gudmundsson, M. T., Högnadóttir, Þ., and Þorkelsson, B.: The 2010 Eyjafjallajökull eruption, Iceland, Report to ICAO, 209p, 2012.

Kristiansen, N., Stohl, A., Prata, A., Bukowiecki, N., Dacre, H., Eckhardt, S., Henne, S., Hort, M., Johnson, B., Marenco, F., et al.: Performance assessment of a volcanic ash transport model mini-ensemble used for inverse modeling of the 2010 Eyjafjallajökull eruption, Journal of Geophysical Research: Atmospheres, 117, 2012.

Lacasse, C. and Garbe-Schönberg, C.-D.: Explosive silicic volcanism in Iceland and the Jan Mayen area during the last 6 Ma: sources and timing of major eruptions, Journal of Volcanology and Geothermal Research, 107, 113–147, 2001.

Larsen, E., Lysså, A., Höskuldsson, Á., Davidsen, J. G., Nadeau, M. J., Power, M., Tassis, G., and Wastegård, S.: A dated volcano-tectonic deformation event in Jan Mayen causing landlocking of Arctic charr, Journal of Quaternary Science, 36, 180–190, 2021.

Larsen, G. and Guðmundsson, M. T.: Catalogue of Icelandic Volcanoes, http://icelandicvolcanoes.is/?volcano=BEE, 2016.

Larsen, G., Gudmundsson, M., and Oladottir, B.: Catalogue of Icelandic Volcanoesn, Report, IMO, UI and CPD-NCIP, 2017.

Macedonio, G., Costa, A., and Folch, A.: Ash fallout scenarios at Vesuvius: numerical simulations and implications for hazard assessment, Journal of Volcanology and Geothermal Research, 178, 366–377, 2008.

Mastin, L. G., Guffanti, M., Servranckx, R., Webley, P., Barsotti, S., Dean, K., Durant, A., Ewert, J. W., Neri, A., Rose, W. I., et al.: A multidisciplinary effort to assign realistic source parameters to models of volcanic ash-cloud transport and dispersion during eruptions, Journal of Volcanology and Geothermal Research, 186, 10–21, 2009.

Mazzocchi, M., Hansstein, F., and Ragona, M.: The 2010 volcanic ash cloud and its financial impact on the European airline industry, in: CESifo Forum, vol. 11, pp. 92–100, München: ifo Institut für Wirtschaftsforschung an der Universität München, 2010.

NavCanada: Polar routes – past, present and future, https://www.navcanada.ca/en/news/blog/polar-routes--past-present-and-future.aspx, 2017.

Newhall, C. G. and Self, S.: The volcanic explosivity index (VEI) an estimate of explosive magnitude for historical volcanism, Journal of Geophysical Research: Oceans, 87, 1231–1238, 1982.

Oxford-economics: The economics impacts of air travel restrictions due to volcanic ash., https://www.oxfordeconomics.com/my-oxford/projects/129051, 2010.

Peron-Pinvidic, G., Gernigon, L., Gaina, C., and Ball, P.: Insights from the Jan Mayen system in the Norwegian–Greenland sea—I. Mapping of a microcontinent, Geophysical Journal International, 191, 385–412, 2012.

Prata, A. T., Dacre, H. F., Irvine, E. A., Mathieu, E., Shine, K. P., and Clarkson, R. J.: Calculating and communicating ensemble-based volcanic ash dosage and concentration risk for aviation, Meteorological Applications, 26, 253–266, 2019.

Pyle, D. M.: Sizes of volcanic eruptions, in: The encyclopedia of volcanoes, pp. 257–264, Elsevier, 2015.

Sandri, L., Costa, A., Selva, J., Tonini, R., Macedonio, G., Folch, A., and Sulpizio, R.: Beyond eruptive scenarios: assessing tephra fallout hazard from Neapolitan volcanoes, Scientific reports, 6, 1–13, 2016.

Siggerud, T.: The volcanic eruption on Jan Mayen 1970, Norsk Polarinstitutt Arbok, 1970, 5–18, 1972.

Stewart-Green, C.: ANS Planning: NAV CANADA, https://www.icao.int/NACC/Documents/Meetings/2016/ASBU/ASBUP12.pdf, 2016.

Sulpizio, R., Folch, A., Costa, A., Scaini, C., and Dellino, P.: Hazard assessment of far-range volcanic ash dispersal from a violent Strombolian eruption at Somma-Vesuvius volcano, Naples, Italy: implications on civil aviation, Bulletin of Volcanology, 74, 2205–2218, 2012.

Suzuki, T. et al.: A theoretical model for dispersion of tephra, Arc volcanism: physics and tectonics, 95, 113, 1983.

Tesche, M., Glantz, P., Johansson, C., Norman, M., Hiebsch, A., Ansmann, A., Althausen, D., Engelmann, R., and Seifert, P.: Volcanic ash over Scandinavia originating from the Grímsvötn eruptions in May 2011, Journal of Geophysical Research: Atmospheres, 117, 2012.

Voelker, A. H. and Haflidason, H.: Refining the Icelandic tephrachronology of the last glacial period–the deep-sea core PS2644 record from the southern Greenland Sea, Global and Planetary Change, 131, 35–62, 2015.

Ward, P. L.: What really causes global warming?: greenhouse gases or ozone depletion?, Morgan James Publishing, 2015.

Woodhouse, M. J., Hogg, A. J., Phillips, J. C., and Rougier, J. C.: Uncertainty analysis of a model of wind-blown volcanic plumes, Bulletin of volcanology, 77, 1–28, 2015.